Vector chiral and multipolar orders in the spin-$\frac{1}{2}$ frustrated ferromagnetic chain in magnetic field

Toshiya Hikihara,[1] Lars Kecke,[2,3] Tsutomu Momoi,[2] and Akira Furusaki[2]
[1]*Department of Physics, Hokkaido University, Sapporo 060-0810, Japan*
[2]*Condensed Matter Theory Laboratory, RIKEN, Wako, Saitama 351-0198, Japan*
[3]*Institut für Theoretische Physik, Universität Ulm, 89069 Ulm, Germany*
(Received 5 July 2008; revised manuscript received 5 September 2008; published 6 October 2008)

We study the one-dimensional spin-1/2 Heisenberg chain with competing ferromagnetic nearest-neighbor J_1 and antiferromagnetic next-nearest-neighbor J_2 exchange couplings in the presence of magnetic field. We use both numerical approaches (the density-matrix renormalization-group method and exact diagonalization) and effective-field-theory approach and obtain the ground-state phase diagram for wide parameter range of the coupling ratio J_1/J_2. The phase diagram is rich and has a variety of phases, including the vector chiral phase, the nematic phase, and other multipolar phases. In the vector chiral phase, which appears in relatively weak magnetic field, the ground state exhibits long-range order (LRO) of vector chirality which spontaneously breaks a parity symmetry. The nematic phase shows a quasi-LRO of antiferronematic spin correlation and arises as a result of formation of two-magnon bound states in high magnetic fields. Similarly, the higher multipolar phases, such as triatic ($p=3$) and quartic ($p=4$) phases, are formed through binding of p magnons near the saturation fields, showing quasi-LRO of antiferromultipolar spin correlations. The multipolar phases cross over to spin-density-wave phases as the magnetic field is decreased before encountering a phase transition to the vector chiral phase at a lower field. The implications of our results to quasi-one-dimensional frustrated magnets (e.g., $LiCuVO_4$) are discussed.

DOI: 10.1103/PhysRevB.78.144404 PACS number(s): 75.10.Jm, 75.10.Pq, 75.40.Cx

I. INTRODUCTION

There is resurgence of theoretical interest in the one-dimensional frustrated ferromagnetic Heisenberg model in magnetic field,[1–9]

$$\mathcal{H} = J_1 \sum_l \boldsymbol{s}_l \cdot \boldsymbol{s}_{l+1} + J_2 \sum_l \boldsymbol{s}_l \cdot \boldsymbol{s}_{l+2} - h \sum_l s_l^z, \tag{1}$$

where the nearest-neighbor exchange is ferromagnetic $J_1<0$, the competing next-nearest-neighbor exchange is antiferromagnetic $J_2>0$, and $\boldsymbol{s}_l$ is a spin-1/2 operator on the site l. The model has recently attracted much attention as it is considered to describe magnetic properties of quasi-one-dimensional edge-sharing chain cuprates, such as $Rb_2Cu_2Mo_3O_{12}$ (Ref. 10) and $LiCuVO_4$.[11] In particular, there have been intensive experimental studies of $LiCuVO_4$, exploring an unusual phase transition in magnetic field from a spiral-ordered phase to a modulated-collinear-ordered phase[12,13] and a multiferroic behavior.[14–16]

From a theoretical point of view, the J_1-J_2 spin chain (1) is of special interest as it is the simplest of the frustrated quantum spin models and provides a good testing ground to look for exotic quantum phases induced by frustration. The theoretical studies over the past several decades have mostly considered the case where both couplings are antiferromagnetic, $J_1>0$ and $J_2>0$. It has been established that in zero magnetic field the ground state of the antiferromagnetic J_1-J_2 spin chain undergoes a phase transition from a critical phase with gapless excitations for $J_2<J_{2c}=0.2411J_1$ to a gapped phase with spontaneous dimerization for $J_2>J_{2c}$ as J_2 increases.[17–23] It has also been revealed that the model exhibits cusp singularities and a 1/3 plateau in the magnetization curve,[24,25] as well as a vector chiral order in the case of anisotropic exchange couplings[26–28] or under magnetic field.[29–32]

In this paper we concentrate on the ferromagnetic case ($J_1<0$) of the J_1-J_2 spin chain (1) in magnetic field which partially polarizes spins to the $+z$ direction. We show that the ground-state phase diagram in the case is a zoo of exotic quantum phases using the numerical density-matrix renormalization-group (DMRG) method,[33–36] exact-diagonalization method, and effective-field theories. We find a phase with long-range vector chiral order and phases with various kinds of multipolar spin correlations, most of which have not been known to appear in this model.

Let us briefly review established results from previous studies on the ferromagnetic J_1-J_2 spin chain and introduce our new findings. In zero field the ground state is ferromagnetic for $J_1/J_2<-4$ and spin singlet for $-4<J_1/J_2<0$; the nature of the spin singlet ground state is not well understood. The ground-state manifold has extensive degeneracy at the phase boundary $J_1/J_2=-4$.[37,38] In magnetic field the spins order with a helical magnetic structure

$$\boldsymbol{s}_l/s = (\sin\theta^c \cos\phi_l^c, \sin\theta^c \sin\phi_l^c, \cos\theta^c) \tag{2}$$

in the classical limit ($s=|\boldsymbol{s}|\gg 1$), with a pitch angle

$$\phi^c = \phi_{l+1}^c - \phi_l^c = \pm \arccos(-J_1/4J_2) \tag{3}$$

and a canting angle

$$\theta^c = \arccos[4hJ_2/s(J_1+4J_2)^2] \tag{4}$$

when $-4<J_1/J_2<0$. One might expect that this helical magnetic order should be completely destroyed by quantum fluctuations in the quantum limit $s=1/2$. It is important to note, however, that a part of the broken symmetries in the classical

helical spin configuration may remain to be spontaneously broken even in the quantum limit. Indeed, the chirality (the sign of ϕ^c) of the helical spin configuration is Z_2 valued and can be broken in (1+1) dimensions. The chirality can be measured with the vector chiral order parameter,

$$\kappa_l^{(n)} = (\boldsymbol{s}_l \times \boldsymbol{s}_{l+n})^z = s_l^x s_{l+n}^y - s_l^y s_{l+n}^x \tag{5}$$

with $n=1$ and 2; its classical value is $\kappa_l^{(n)} = s^2 \sin^2 \theta^c \sin(n\phi^c)$. In this paper we show that the vector chirality $\kappa_l^{(n)}$ is long-range ordered in the weak-field regime of the phase diagram of the ferromagnetic J_1-J_2 model.[39] We also show that the vector chiral order parameters satisfy the relation

$$J_1 \langle \kappa_l^{(1)} \rangle + 2J_2 \langle \kappa_l^{(2)} \rangle = 0, \tag{6}$$

where $\langle \cdots \rangle$ denotes average in the ground state. This implies that the spin current, $J_{ij}(\boldsymbol{s}_i \times \boldsymbol{s}_j)^z$, flowing on the link connecting the sites i and j ($J_{ij}=J_1$ or J_2) is confined and circulating in each triangle made of the three neighboring sites. Incidentally, we note that the classical helical configuration (2) satisfies Eq. (6).

Vector chirality (5) is an antisymmetric product of two spin-1/2 operators. This is an example of the $\boldsymbol{p}$-type nematic operator introduced by Andreev and Grishchuk.[40] In this paper, we shall reserve the term "nematic" for symmetric products (termed $\boldsymbol{n}$ type in Ref. 40) and call the antisymmetric product (5) the vector chirality. Examples of what we call nematic operators are

$$Q_{x^2-y^2} = s_i^x s_j^x - s_i^y s_j^y, \quad Q_{xy} = s_i^x s_j^y + s_i^y s_j^x, \tag{7}$$

which can be thought of as members of quadrupolar spin operators.

Interestingly enough, the phase diagram of the ferromagnetic J_1-J_2 spin chain has a Tomonaga-Luttinger (TL) liquid phase with quasi-long-range antiferronematic order $Q_{--} = Q_{x^2-y^2} - iQ_{xy} = s_i^- s_j^-$, where $s_j^- = s_j^x - is_j^y$. As first pointed out by Chubukov,[1] this nematic order is realized due to pairing of two-magnon excitations. The paired magnons are the low-energy excitations of the TL liquid with the nematic quasi-long-range order. This was confirmed recently by numerical calculation of nematic correlation function at $J_1/J_2=-1$.[7] In this paper we explore wider region of the parameter space and show that the nematic TL-liquid phase occupies a large part of the phase diagram.

One can generalize the quadrupolar spin orders to higher multipolar orders. For example, one can define octupolar triatic order[41] $O_{---} = O_{x^3-3xy^2} + iO_{y^3-3x^2y} = s_i^- s_j^- s_k^-$ with

$$O_{x^3-3xy^2} = s_i^x s_j^x s_k^x - s_i^x s_j^y s_k^y - s_i^y s_j^x s_k^y - s_i^y s_j^y s_k^x, \tag{8a}$$

$$O_{y^3-3x^2y} = s_i^y s_j^y s_k^y - s_i^y s_j^x s_k^x - s_i^x s_j^y s_k^x - s_i^x s_j^x s_k^y, \tag{8b}$$

and, similarly, the hexadecapolar order $H_{----} = H_{x^4-6x^2y^2+y^4} - iH_{x^3y-xy^3} = s_i^- s_j^- s_k^- s_l^-$, which we dub the "quartic" order, and so on. In fact, signatures of binding of three or four magnons are found in recent numerical studies of magnetization curves[2,3] and of multimagnon instabilities at a saturation field.[6] In this paper we establish the existence of TL-liquid phases with the triatic and quartic orders through the DMRG calculation of correlation functions. It is interesting to note that quasi-long-range molecular superfluid phases (called trionic and quartetting phases), similar to the above-mentioned triatic and quartic phases, have recently been found in a model of one-dimensional multicomponent fermionic cold atoms.[42–44]

This paper is organized as follows. In Sec. II we present the ground-state phase diagram and briefly describe properties of the phases identified in the present work. These are vector chiral, nematic, incommensurate nematic, triatic, quartic phases, and spin-density-wave phases (SDW_2 and SDW_3). This section gives a summary of the main results of the paper. In Sec. III we consider formation of multimagnon bound states which destabilizes the fully polarized state. The results of this consideration allow us to determine phases emerging just below the saturation field. In Sec. IV we study magnetization process of model (1) for several values of the ratio J_1/J_2 and find a transition from a single-spin-flip process to a multi-spin-flip process. The transition point is identified as the boundary of the vector chiral phase in the phase diagram. The remaining sections present detailed analysis of correlation functions in each phase, which we calculate using the DMRG method. In Sec. V, we consider the vector chiral phase. After a brief review of bosonization approach due to Kolezhuk and Vekua[29] which is valid for $|J_1| \ll J_2$, numerical results of the DMRG calculation are presented. In Sec. VI we discuss the nematic phase. We introduce a hard-core Bose gas of two-magnon bound states as an effective theory for the nematic phase. We find good agreement between the theory and numerics of various correlation functions in the nematic phase. In Sec. VII we show our numerical results for the incommensurate nematic phase, which exhibits quasi-long-range order of the nematic correlation with an incommensurate wave number. In Sec. VIII we apply the hard-core boson theory to the triatic and quartic phases. We show that these phases can be understood as TL liquids of hard-core bosons which correspond to three- and four-magnon bound states, respectively, just as the nematic phase is a TL liquid of two-magnon bound states. We conclude with some remarks in Sec. IX. Relation (6) is derived in Appendix.

II. PHASE DIAGRAM

The ground-state phase diagram obtained in the present work is summarized in Fig. 1 in the planes of (a) J_1/J_2 versus h/J_2 and (b) J_1/J_2 versus the magnetization per site M. The phase diagram contains (at least) eight phases: vector chiral (VC) phase, nematic (N) phase, incommensurate nematic (IN) phase, triatic (T) phase, quartic (Q) phase, two kinds of spin-density-wave phases (SDW_2 and SDW_3), and ferromagnetic (F) phase. Brief explanation of these phases is given below. More detailed discussions on each phase will be given in Secs. V–VIII. Figure 2 shows typical spatial dependence of various correlation functions in these phases.

Ferromagnetic phase. In the ferromagnetic phase, spins are fully polarized, $M=1/2$. This phase is stable when $J_1/J_2<-4$ or when large enough magnetic field is applied. We will discuss in Sec. III magnetic instabilities along the phase boundary of the ferromagnetic phase.

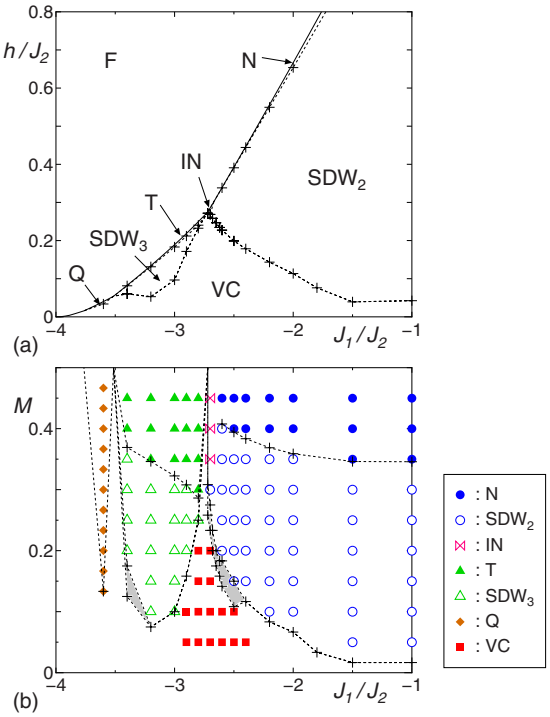

FIG. 1. (Color online) Magnetic phase diagram of the spin-1/2 zigzag chain with ferromagnetic J_1 and antiferromagnetic J_2 (a) in the J_1/J_2 versus h/J_2 plane and (b) in the J_1/J_2 versus M plane. Crosses show the transition and crossover points obtained from the magnetization curves and correlation functions. In (a), symbols VC, N, IN, T, Q, and F indicate the vector chiral ($\Delta S^z_{\rm tot}=1$), nematic ($\Delta S^z_{\rm tot}=2$), incommensurate nematic ($\Delta S^z_{\rm tot}=2$), triatic ($\Delta S^z_{\rm tot}=3$), quartic ($\Delta S^z_{\rm tot}=4$), and ferromagnetic (fully polarized) phases, respectively. Here $\Delta S^z_{\rm tot}$ is the unit of changes in the total $S^z_{\rm tot}=\Sigma_l s^z_l$ when the magnetic field h is swept. There are also two kinds of spin-density-wave phases: SDW_2 ($\Delta S^z_{\rm tot}=2$) and SDW_3 ($\Delta S^z_{\rm tot}=3$), which are related to the nematic and triatic phases, respectively. The solid curve shows the saturation field h_s and dotted lines are the guide for the eyes. In (b), symbols indicate parameter points for which their ground-state phase is identified by analysis of correlation functions. Shaded regions in (b) correspond to the magnetization jump at the first-order transition (see Sec. IV).

Vector chiral phase. The vector chiral phase appears in small magnetic field. This phase is characterized by long-range order of the vector chiral correlation (5). The ground state breaks a Z_2 symmetry as Eq. (5) indicates that the parity about a bond center is broken spontaneously. We can also regard this Z_2-symmetry breaking as choosing one of the two possible directions of circulation of spontaneous s^z-spin current flow. A schematic picture of the vector chiral order and circulating spin current in the Z_2-symmetry broken state is shown in Fig. 3, where the spin chain is drawn as a zigzag ladder. Numerical evidence for the long-range order will be presented in Sec. V. Another important feature of the vector chiral phase is that the transverse-spin correlation $\langle s^x_0 s^x_l\rangle$ is incommensurate with the lattice and stronger than the longitudinal correlation $\langle s^z_0 s^z_l\rangle - \langle s^z_0\rangle\langle s^z_l\rangle$.

Nematic/SDW$_2$ phases. At higher magnetic field up to the saturation field, the nematic/SDW_2 phases[1,6,7,40] appear at $J_1/J_2 \gtrsim -2.7$. These phases are a TL liquid of hard-core bosons which are actually two-magnon bound states with total momentum $k=\pi$. The boson creation operator $b^\dagger_l$ corresponds to $s^-_l s^-_{l+1}$ and the boson density $n_l = b^\dagger_l b_l \propto \frac{1}{2} - s^z_l$. Since breaking a two-magnon bound-state costs a finite binding energy, the transverse-spin correlation $\langle s^+_0 s^-_l\rangle$ is short ranged, where $s^+_0 = s^x_0 + i s^y_0$. Being a TL liquid, the ground state exhibits power-law decaying correlations of the single-boson propagator, $\langle b_0 b^\dagger_l\rangle \propto \langle s^+_0 s^+_1 s^-_l s^-_{l+1}\rangle$, and the density fluctuations, $\langle n_0 n_l\rangle - \langle n_0\rangle\langle n_l\rangle \propto \langle s^z_0 s^z_l\rangle - \langle s^z_0\rangle\langle s^z_l\rangle$. When the boson propagator decays slower than the density-density correlation, it is appropriate to call this phase the (spin) nematic phase. In the opposite case when the latter incommensurate density correlation is dominant, we call this phase the spin-density-wave (SDW_2) phase. The SDW_2 phase is extended to the antiferromagnetic side $J_1>0$ across the decoupled-chain limit $J_1=0$; it is called even-odd phase in Ref. 25. The boundary between the SDW_2 phase and the nematic phase is shown by a dotted line in Fig. 1.

In the semiclassical picture we can write $s^-_l = e^{-i\phi_l}$, where ϕ_l is the angle of the two-dimensional vector (s^x_l, s^y_l) measured from the positive x direction, $0 \le \phi_l < 2\pi$. The product $s^-_l s^-_{l+1} = e^{-i(\phi_l+\phi_{l+1})}$ can be represented by the vector $\boldsymbol{N}_{l+1/2} = (\cos\Phi_{l,2}, \sin\Phi_{l,2})$ with $\Phi_{l,2} = -(\phi_l+\phi_{l+1})/2$. We now realize that we need to identify $\boldsymbol{N}_{l+1/2}$ with $-\boldsymbol{N}_{l+1/2}$ because of the physical identification $(\phi_l, \phi_{l+1}) \equiv (\phi_l + 2\pi, \phi_{l+1}) \equiv (\phi_l, \phi_{l+1} + 2\pi)$. We can thus consider $\boldsymbol{N}_{l+1/2}$ as a director representing the nematic order. We will show in Sec. VI that the nematic phase has antiferronematic quasi-long-range order of the director, as shown schematically in Fig. 4. The ground state is not dimerized in this phase as opposed to the initial proposal of Chubukov.[1]

Incommensurate nematic phase. The incommensurate nematic phase occupies a very small region in the phase diagram. This phase has quasi-long-range order of the nematic correlation with an incommensurate wave number. The correlation is due to two-magnon bound states with momentum $k=\pi+\delta$ and $\pi-\delta$ instead of $k=\pi$ in the nematic phase. Schematic pictures of the incommensurate nematic order are depicted in Fig. 5, where the upper and lower pictures represent the nematic correlation with wave number $k=\pi+\delta$ and $\pi-\delta$, respectively. If the densities of paired magnons with $k=\pi+\delta$ and $\pi-\delta$ are different, one of the two correlation patterns in Fig. 5 becomes dominant, and the Z_2 chiral symmetry is broken spontaneously, as suggested by Chubukov.[1] However, we have found no signature of long-range order of the chiral correlation in our numerical calculation, which we will discuss in Sec. VII.

Triatic and SDW$_3$ phases. The triatic phase exists below the saturation field and next to the incommensurate nematic phase. The triatic/SDW_3 phases are a TL liquid of bosons which represent three-magnon bound states with total momentum $k=\pi$. In analogy with the nematic phase, the triatic order has a simple semiclassical picture. Writing the bound three magnons as $s^-_l s^-_{l+1} s^-_{l+2} = e^{-i(\phi_l+\phi_{l+1}+\phi_{l+2})} = e^{3i\Phi_{l,3}}$, we may consider the triatic order as ordering of the angle $\Phi_{l,3} = -(\phi_l+\phi_{l+1}+\phi_{l+2})/3$, which has the property $\Phi_{l,3} \equiv \Phi_{l,3} + 2\pi/3$. A schematic picture of the triatic ordered state is shown in Fig. 6. In the triatic phase, correlation functions probing three-magnon bound states, such as $\langle s^+_0 s^+_1 s^+_2 s^-_l s^-_{l+1} s^-_{l+2}\rangle$, exhibit quasi-long-range order (power-law

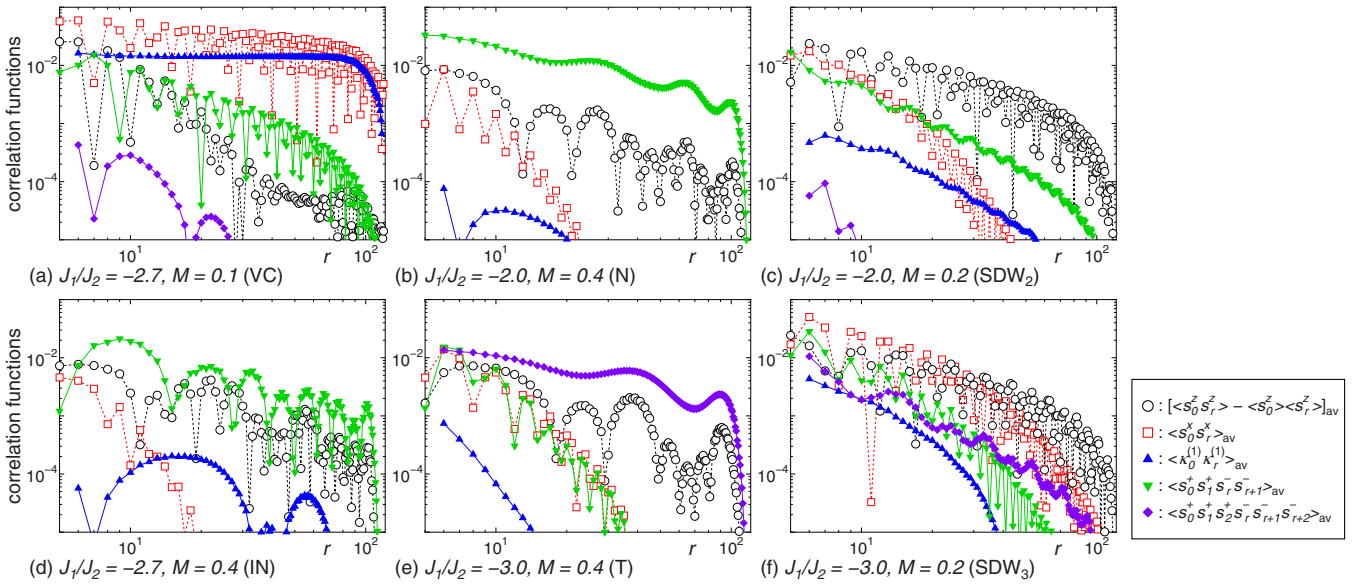

FIG. 2. (Color online) Typical behaviors of various correlation functions in (a) the vector chiral (VC) phase, (b) the nematic (N) phase, (c) the SDW$_2$ phase, (d) the incommensurate nematic (IN) phase, (e) the triatic (T) phase, and (f) the SDW$_3$ phase. Absolute values of spatially averaged correlation functions are plotted. (For the averaging procedure, see Sec. V B.) In (b) and (d), the triatic correlation function $\langle s_0^+ s_1^+ s_2^+ s_r^- s_{r+1}^- s_{r+2}^-\rangle_{\rm av}$ is smaller than 10^{-5}.

decay). In contrast, both the transverse-spin correlation $\langle s_0^+ s_l^-\rangle$ and the nematic correlation $\langle s_0^+ s_1^+ s_l^- s_{l+1}^-\rangle$ are short ranged because of a finite-energy cost for breaking a three-magnon bound state. The longitudinal-spin correlation $\langle s_0^z s_l^z\rangle - \langle s_0^z\rangle\langle s_l^z\rangle$ shows algebraic decay, as s_l^z is related to the boson density. When the most slowly decaying correlation is the longitudinal-spin correlation, we call the phase the SDW$_3$ phase. The boundary between the triatic phase and the SDW$_3$ phase is shown by a dotted curve in Fig. 1. The detailed discussion of the correlation functions will be given in Sec. VIII.

Quartic phase. The quartic phase is a TL-liquid phase of four-magnon bound states with momentum $k=\pi$. Its properties can be easily deduced by straightforward generalization from the triatic phase.

III. MULTIMAGNON INSTABILITY

We begin our study of the phase diagram by examining instabilities of the fully polarized state. To that end, we numerically calculate energy dispersion of low-energy excitations with a small number of magnons (down spins). The analysis presented here extends the result reported in our previous study.[6]

Inside the ferromagnetic phase in magnetic field, there is a finite-energy gap between the ground state and excited states. With decreasing the magnetic field, the gap becomes smaller and eventually vanishes at the boundary of the ferromagnetic phase. We define the saturation field h_s as the magnetic field h at which a branch of excitations first becomes gapless as the field h is reduced. In the ferromagnetic J_1-J_2 spin chain, the excitation mode that becomes gapless (soft) at $h=h_s$ is *a multimagnon bound state*. Below the saturation field the soft multimagnon bound states proliferate. As a result the ground state can change into a TL liquid with the correlation that is represented by the soft bound multimagnon mode. It is therefore important to find out which branch of multimagnon bound states is the soft mode.

We calculate energy of p-magnon excitations using the method we introduced in Ref. 6. The number of magnons p and the total momentum k are good quantum numbers of Hamiltonian (1). We thus expand eigenstates in the sector of p magnons with the basis

$$|p,k;\{r_1,\ldots,r_{p-1}\}\rangle = \frac{1}{\sqrt{\Omega}}\sum_{l=1}^{\Omega}\prod_{n=1}^{p} e^{ikl_n/p} s_{l_n}^- |\mathrm{FM}\rangle, \qquad (9)$$

where

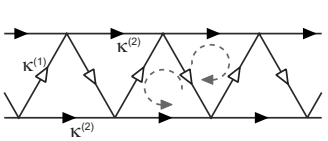

FIG. 3. Schematic picture of the vector chiral order. The arrows on bonds indicate breaking of the parity symmetry by the vector chiral order $\kappa_l^{(n)}=(\boldsymbol{s}_l\times\boldsymbol{s}_{l+n})^z$, which obeys the relation $J_1\langle\kappa^{(1)}\rangle + 2J_2\langle\kappa^{(2)}\rangle=0$. The circulation of the s^z spin current, shown by the dashed arrows, is alternating, and there is no net spin current flow.

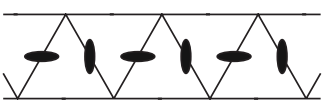

FIG. 4. Schematic picture of antiferronematic quasi-long-range order in the nematic phase. Ellipses represent directors of the nematic order on each bond.

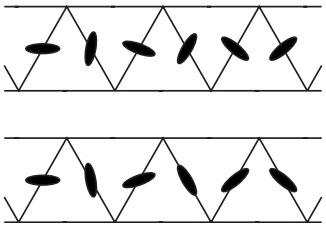

FIG. 5. Schematic pictures of incommensurate nematic quasi-long-range order in the incommensurate *chiral* nematic phase. Ellipses represent directors of the nematic order on each bond. The numerical results in Sec. VII indicate that this chiral symmetry is not broken in the incommensurate nematic phase; the ground state is given by equal superposition of the upper and lower configurations.

$$l_n = l + \sum_{i=1}^{n-1} r_i. \tag{10}$$

Here $|\mathrm{FM}\rangle$ is the fully polarized state ($s_i^+|\mathrm{FM}\rangle=0$), Ω is the system size taken to be $\Omega\to\infty$, and r_i $(1\le i\le p-1)$ is the distance between the ith and $(i+1)$th magnons. The periodic boundary condition is imposed in this calculation. We take r_i to be in the range of $1\le r_i\le r_{\max}$, where $r_{\max}$ is chosen so that wave-function vectors can be stored in the computer memory. (The finite value of $r_{\max}$ limits the accuracy of energy calculations. For tightly bound magnons, errors caused by this approximation can be made negligibly small on the order of exponentially decaying tails of their wave function.)

We numerically diagonalize the Hamiltonian matrix expressed in the restricted Hilbert space ($r_i\le r_{\max}$) and obtain the lowest energy as a function of the total momentum k for each p magnon sector. In this way we obtain energy dispersion of p-magnon bound states. In our previous study[6] we calculated energy dispersion of multimagnon excitations for up to $p=4$. Here we extend the calculation to include more magnons ($p_{\max}=8$), taking the maximum distance $r_{\max}$ to be at least $42/(p-1)$. We thereby identify soft multimagnon modes and determine the saturation field h_s at each value of the ratio J_1/J_2 $(-4<J_1/J_2<0)$.

Table I summarizes the number of magnons p and the momentum k of the multimagnon modes ($p\le 8$) which become gapless at the saturation field. We note that the gapless modes with $p\le 4$ in Table I are soft modes giving rise to multipolar TL liquids, since non-negative excitation energy of $2p$-magnon modes indicates a repulsive interaction between bound p magnons (see the discussion at the end of this section). We thus find that, as Chubukov[1] first pointed out, the two-magnon bound state with $k=\pi$ is the soft mode when $-2.669<J_1/J_2<0$. Its exact wave function can be easily obtained; it turns out that the bound-state wave function at $k=\pi$ has amplitudes only for odd integer values of r_1, which means that the magnons forming a bound pair are on different legs of the zigzag ladder. The soft mode signals emergence of a nematic phase below the saturation field.

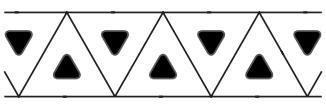

FIG. 6. Schematic picture of antiferrotriatic quasi-long-range order in the triatic phase. Solid triangles represent spin structure of the triatic order formed by three $s=1/2$ spins on each plaquette.

TABLE I. Number of magnons p and total momentum k of the multimagnon bound states which become gapless at the saturation field.

Parameter range	p	k
$-2.669<J_1/J_2<0$	2	π
$-2.720<J_1/J_2<-2.669$	2	$\pi\pm\delta$ $(\delta>0)$
$-3.514<J_1/J_2<-2.720$	3	π
$-3.764<J_1/J_2<-3.514$	4	π
$-3.888<J_1/J_2<-3.764$	5	π
$-3.917<J_1/J_2<-3.888$	6	π
$-4<J_1/J_2<-3.917$	7	π

In the narrow range $-2.720<J_1/J_2<-2.669$, the soft two-magnon bound state has an incommensurate momentum $k\neq\pi$. Our numerical estimate of the commensurate-incommensurate transition point is consistent with the exact result, $(J_1/J_2)_c=-2.669\,08\cdots$.[5] Beyond the commensurate-incommensurate transition point, the total momentum k changes continuously as $k/\pi=1-0.67\sqrt{(J_1/J_2)_c-J_1/J_2}$ (see Fig. 7). This suggests continuous nature of the transition between the commensurate and incommensurate nematic phases at $h=h_s$.

As the ratio J_1/J_2 is changed toward the end point at $J_1/J_2=-4$, the magnon number p of the lowest bound-magnon branch increases (see Table I). The total momentum of the bound-magnon mode is always at $k=\pi$, except in the narrow region of the incommensurate two-magnon bound states mentioned above. We expect that many-magnon bound states, formed by more than seven magnons, should appear as $J_1/J_2\to-4$. In our numerical calculation, eight-magnon bound states did not come down as the lowest state, which we suspect was due to finite-size effects coming from small $r_{\max}$.

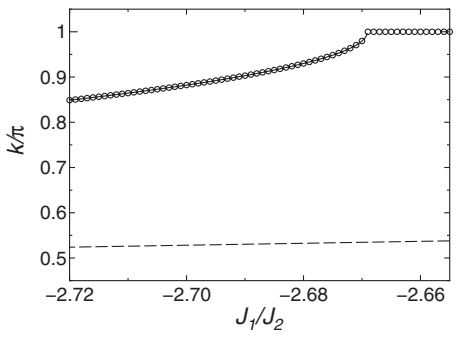

FIG. 7. Dependence on J_1/J_2 of the center-of-mass momentum k for the two-magnon bound state. The momentum deviates continuously from π at $J_1/J_2\simeq-2.669$. The incommensurate momentum k is fitted well to $k/\pi=1-0.67\sqrt{-2.669-J_1/J_2}$ as shown by the solid curve. The dashed line is the classical estimate $k=2\arccos(-J_1/4J_2)$ for two scattering magnons.

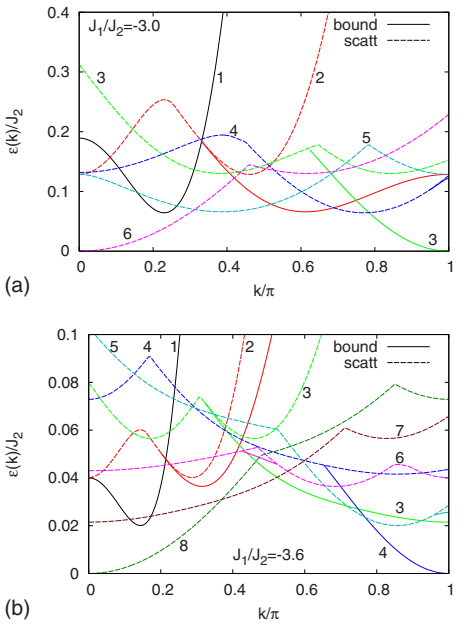

FIG. 8. (Color online) Dispersion curves of multimagnon bands at the saturation field for (a) $J_1/J_2=-3.0$ and (b) $J_1/J_2=-3.6$. The solid curves are the dispersions of bound states and the dashed curves show the lower edges of the continuum of scattering states. For clarity, only the states of up to six magnons are shown in (a) and up to eight magnons in (b). The numbers printed beside the curves denote the number of magnons. Bound states inside the scattering continuum are not shown.

To demonstrate stability of the multimagnon bound states, we show in Fig. 8 dispersion curves of bound-magnon excitations, as well as lower edges of continuous spectra of magnon scattering states, at the saturation field $h=h_s$ for $J_1/J_2=-3.0$ and -3.6. The p-magnon scattering states are constructed from a set of one-, two-, …, $(p-1)$-magnon (bound) states in total of p magnons. At $J_1/J_2=-3.0$ [Fig. 8(a)], the three-magnon bound state is gapless at $k=\pi$. The branches of one, two, four, and five magnons have finite excitation gaps. This feature is consistent with a finite binding energy of the three-magnon bound state. Furthermore, the state with the lowest energy (at $k=0$) in the six-magnon sector belongs to the continuum of scattering states formed by a pair of three-magnon bound states. This indicates that three-magnon bound states are interacting repulsively with each other. The repulsive interaction rules out the possibility of a metamagnetic transition (magnetization jump) at the saturation field and instead induces a continuous transition to the triatic phase which we discuss in more detail in Sec. VIII. The multimagnon dispersions for $J_1/J_2=-3.6$, shown in Fig. 8(b), can also be understood in the same fashion. Here it is the four-magnon bound states that become gapless at the saturation field. The instability of the fully polarized state is driven by the four-magnon bound states with mutual repulsive interactions, which condense to form a TL liquid with quartic order, as we will show in Sec. VIII.

IV. MAGNETIZATION CURVE

Having identified the soft modes at the saturation field $h=h_s$, we now study magnetization process of spin chains of

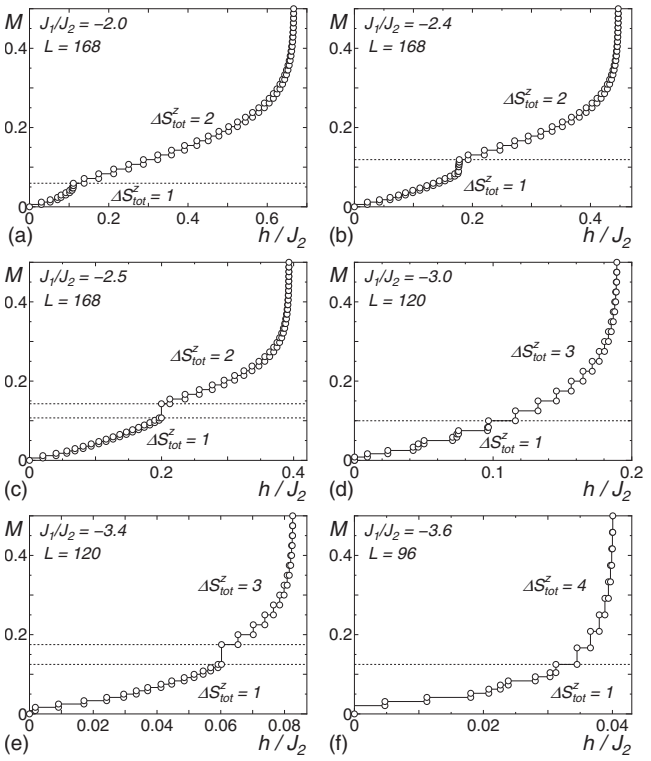

FIG. 9. Magnetization curves for (a) $J_1/J_2=-2.0$, (b) $J_1/J_2=-2.4$, (c) $J_1/J_2=-2.5$, (d) $J_1/J_2=-3.0$, (e) $J_1/J_2=-3.4$, and (f) $J_1/J_2=-3.6$. The dotted lines represent the boundaries of the regions of $\Delta S^z_{\rm tot}=1$ and $\Delta S^z_{\rm tot}\geq 2$.

finite length, which we obtain numerically for various values of the coupling ratio J_1/J_2. The numerical results help us to deduce overall structure of the magnetic phase diagram. Previous studies[2,3] have found that, near the saturation field, the total magnetization $S^z_{\rm tot}=\Sigma_l s^z_l$ changes in units of $\Delta S^z_{\rm tot}=2$, 3, and 4 for $J_1/J_2\gtrsim -2.6$, $-3\leq J_1/J_2\leq -2.8$, and $J_1/J_2=-3.75$, respectively. The multi-spin-flip is a natural consequence of the formation of stable multimagnon bound states. At lower fields $S^z_{\rm tot}$ changes by $\Delta S^z_{\rm tot}=1$.

We obtain magnetization curves from the following procedure. With the DMRG method we calculate the lowest energy $E_0(M)$ of model (1) at $h=0$ in each Hilbert subspace of magnetization per site $M=S^z_{\rm tot}/L$, where L is the number of total sites. The magnetization curve $M(h)$ is then obtained by finding the magnetization M which minimizes $E_0(M)-hS^z_{\rm tot}$ for given h. We have performed the calculation for open chains of up to $L=168$ sites. We kept up to 350 states in our DMRG calculation.

Figure 9 shows representative magnetization curves calculated at various values of J_1/J_2. We clearly see that the total magnetization $S^z_{\rm tot}$ changes by $\Delta S^z_{\rm tot}=1$ at low magnetic fields, while it shows multi-spin-flip process $\Delta S^z_{\rm tot}\geq 2$ at higher fields. The magnetization change in the high-field regime is $\Delta S^z_{\rm tot}=2$ for $J_1/J_2\geq -2.7$, $\Delta S^z_{\rm tot}=3$ for $-3.4\leq J_1/J_2\leq -2.75$, and $\Delta S^z_{\rm tot}=4$ at $J_1/J_2=-3.6$. These features of the magnetization process are consistent with our finding of stable multimagnon bound states discussed in Sec. III. The critical field h_c and the critical magnetization M_c, at which the magnetization step changes from $\Delta S^z=1$ to $\Delta S^z>1$, are

plotted in the phase diagram shown in Fig. 1.

The magnetic phase diagram (Fig. 1) has four distinct regions characterized by $\Delta S^z_{\rm tot}=1$, 2, 3, and 4. These regions correspond to the vector chiral, nematic or SDW_2, triatic or SDW_3, and quartic phases, respectively. We will discuss each region in detail in Secs. V–VIII. The phase boundary between the region of $\Delta S^z_{\rm tot}=1$ and that of $\Delta S^z_{\rm tot}=2$ begins from the critical coupling $J_1/J_2=-2.72$ at $h=h_s$, which is the phase boundary between the incommensurate nematic and triatic phases,[6] and appears to go toward small $|J_1|/J_2$ region as h is decreased.

When $-2.72<J_1/J_2\leq -2.5$, the magnetization curve exhibits a large jump (of order L^0) on the phase boundary between the region of $\Delta S^z_{\rm tot}=1$ and that of $\Delta S^z_{\rm tot}=2$, whereas for $J_1/J_2\geq -2.4$ the magnetization curve appears to become continuous (i.e., steps are of order L^{-1}). Similarly, we observed a large jump in the magnetization between the $\Delta S^z_{\rm tot}=1$ and $\Delta S^z_{\rm tot}=3$ regions at $J_1/J_2=-3.4$ but not at other values. However, we find that the magnetization curve at $J_1/J_2=-2.4$ also develops a sharper change at $M=M_c$ with increasing the system size L, which turns into almost a discontinuous jump at $L=168$ [see Fig. 9(b)]. This may suggest that the transition becomes first order at $L\to\infty$. Since we do not have a good scheme of extrapolation to $L\to\infty$ for incommensurate values of M, it is difficult to determine the order of the transition from the numerical calculation alone. More elaborated treatments, especially analytical ones, would be required for resolving this issue.

For the parameters calculated, $J_1/J_2\geq -3.6$, we find that at the saturation field $h=h_s$ the magnetization curve approaches $M=1/2$ continuously in accordance with the previous studies[2,3,6] (see also note added). We note that the square-root singularity $1/2-M\propto(h_s-h)^{1/2}$ is commonly expected for a continuous transition at the saturation field, where soft excitations are described as free hard-core bosons or free fermions.

V. VECTOR CHIRAL PHASE

In this section we take a detailed look at correlation functions in the vector chiral phase. We will show that this phase corresponds to the low-field regime where the magnetization curve has $\Delta S^z_{\rm tot}=1$ steps, and the ground state exhibits a long-range order of the longitudinal vector chirality, $\langle\kappa_l^{(n)}\rangle=\langle(\boldsymbol{s}_l\times\boldsymbol{s}_{l+n})^z\rangle\neq 0$ $(n=1,2)$. We first give a brief review of a low-energy field theory for the vector chiral phase. We then present numerical DMRG results and compare them with the theory.

A. Bosonization approach for $|J_1|\ll J_2$

A field theoretical approach to the vector chiral phase in the J_1-J_2 model was developed by Nersesyan *et al.* in Ref. 26, in which the antiferromagnetic J_1-J_2 chain with easy-plane anisotropy was considered. Kolezhuk and Vekua extended this theory to include effects of the external magnetic field in Ref. 29. Here we follow their approach and apply it to the ferromagnetic J_1-J_2 chain. The theory is based on bosonization of the antiferromagnetic Heisenberg spin chain and perturbative renormalization-group (RG) analysis valid for $|J_1|\ll J_2$.

In the limit $|J_1|\ll J_2$, model (1) can be regarded as two antiferromagnetic Heisenberg spin chains which are weakly coupled by the ferromagnetic interchain interaction J_1. Therefore, we apply the standard bosonization technique to the two chains separately, treating the interchain coupling J_1 as a weak perturbation. The low-energy physics of the Heisenberg chains $(n=1,2)$ is described by free bosonic fields (ϕ_n,θ_n) satisfying the equal-time commutation relation $[\phi_n(x),\partial_y\theta_{n'}(y)]=i\delta(x-y)\delta_{n,n'}$. The spin operators $\boldsymbol{s}_l$ on the site $l=2j+n$ $(j\in\mathbb{Z})$ in Hamiltonian (1) are expressed in terms of the bosonic fields as

$$s^z_{2j+n}=M+\frac{1}{\sqrt{\pi}}\frac{d\phi_n(x_n)}{dx}-(-1)^j a\,\sin[2\pi Mj+\sqrt{4\pi}\phi_n(x_n)]+\cdots, \tag{11}$$

$$s^+_{2j+n}=(-1)^j b e^{i\sqrt{\pi}\theta_n(x_n)}+b' e^{i\sqrt{\pi}\theta_n(x_n)}\sin[2\pi Mj+\sqrt{4\pi}\phi_n(x_n)]+\cdots, \tag{12}$$

where a, b, and b' are nonuniversal constants.[45,46] We have introduced the continuous space coordinate x, on which the bosonic fields depend. On the lattice site $l=2j+n$ the coordinate x takes the value $x_1=j-1/4$ and $x_2=j+1/4$. Equations (11) and (12) allow us to write the interchain interaction in terms of the bosonic fields. The resulting effective Hamiltonian is given by[29]

$$\tilde{\mathcal{H}}=\sum_{\nu=\pm}\frac{v_\nu}{2}\int dx\left[K_\nu\left(\frac{d\theta_\nu}{dx}\right)^2+\frac{1}{K_\nu}\left(\frac{d\phi_\nu}{dx}\right)^2\right]+g_1\int dx\,\sin(\sqrt{8\pi}\phi_-+\pi M)+g_2\int dx\frac{d\theta_+}{dx}\sin(\sqrt{2\pi}\theta_-) \tag{13}$$

with

$$g_1=J_1a^2\sin(\pi M),\quad g_2=\frac{J_1}{2}\sqrt{2\pi}b^2. \tag{14}$$

Here we have introduced bosonic fields for symmetric (+) and antisymmetric (−) sectors, $\phi_\pm=(\phi_1\pm\phi_2)/\sqrt{2}$, $\theta_\pm=(\theta_1\pm\theta_2)/\sqrt{2}$. In lowest order in J_1 the TL-liquid parameters $K_\pm$ and the renormalized spin velocities $v_\pm$ are given by[29]

$$K_\pm=K\left(1\mp J_1\frac{K}{\pi v}\right), \tag{15}$$

$$v_\pm=v\left(1\pm J_1\frac{K}{\pi v}\right), \tag{16}$$

where K and v are, respectively, the TL-liquid parameter and the spin velocity of the decoupled antiferromagnetic Heisenberg spin chains. The TL-liquid parameter K is a function of M increasing monotonically from $K(M=0)=1/2$ to $K(M=1/2)=1$.[47–49] In the weak-coupling limit the velocity v is of order J_2, except near the saturation limit $M\to\frac{1}{2}$, where

$v \to 0$ and the bosonization approach breaks down.

As we can see from Eqs. (11) and (12), the g_1 (g_2) term in Eq. (13) originates from the longitudinal (transverse) part of the interchain exchange coupling. These coupling constants are renormalized as energy scale is decreased in RG transformation. The low-energy physics of the effective Hamiltonian (13) is then determined by the strongest of the renormalized coupling constants. In case the g_1 term is most relevant, the ϕ_- field is pinned at a value which minimizes $g_1 \sin(\sqrt{8\pi}\phi_- + \pi M)$. The resulting ground state is in the nematic phase, as we will discuss in Sec. VI. The vector chiral phase arises when the g_2 coupling is most relevant and renormalized to strong coupling first.

The scaling dimensions of the g_1 and g_2 terms are equal to $2K_-$ and $1+(2K_-)^{-1}$, respectively, at $J_1=0$. It is then natural to expect that the g_2 term can dominate over the g_1 term only in high fields [i.e., for $K_- > (1+\sqrt{5})/4$] when $|J_1| \ll J_2$.[29] However, as we discussed in Sec. III the two-magnon pairing is the strongest instability at $h=h_s$, which favors the nematic order near the saturation field (Fig. 1 and Table I). In fact, the vector chiral phase is found to be realized in the weak-field regime where the bare value of the coupling g_1 is very small ($M \ll 1$) and where the classical value of the vector chirality is larger ($\theta^c \approx \pi/2$).

In the following discussion let us assume that the renormalized g_2 is the largest coupling. In this case we may employ the mean-field decoupling scheme introduced by Nersesyan *et al.*,[26] whose conclusions have been confirmed by numerical studies.[27,28,30–32] In this scheme we assume that both $d\theta_+/dx$ and $\sin(\sqrt{2\pi}\theta_-)$ acquire finite expectation values so that the g_2 term is minimized. We have essentially two choices,

$$\langle \theta_- \rangle = + \sqrt{\frac{\pi}{8}}, \quad \left\langle \frac{d\theta_+}{dx} \right\rangle = + \sqrt{\frac{2}{\pi}}(\pi - 2Q), \tag{17a}$$

and

$$\langle \theta_- \rangle = - \sqrt{\frac{\pi}{8}}, \quad \left\langle \frac{d\theta_+}{dx} \right\rangle = - \sqrt{\frac{2}{\pi}}(\pi - 2Q), \tag{17b}$$

where Q is an incommensurate wave number in the transverse-spin correlation ($0 < Q < \pi/2$) [see Eq. (21)]. Note that $\langle \theta_- \rangle$ and $\langle d\theta_+/dx \rangle$ have the same sign in the frustrated ferromagnetic chain $J_1 < 0$. The Z_2 symmetry is spontaneously broken when the ground state selects one of the two choices in Eqs. (17a) and (17b).

Once the mean-field decoupling is made, the excitations in the antisymmetric sector (ϕ_-, θ_-) acquire a finite-energy gap, and the field ϕ_-, which is dual to the pinned field θ_-, fluctuates strongly. Therefore the g_1 term can be safely ignored. The symmetric sector (ϕ_+, θ_+) is governed by the Gaussian model,

$$\mathcal{H}_+ = \frac{v_+}{2} \int dx \left[K_+ \left(\frac{d\theta_+}{dx} \right)^2 + \frac{1}{K_+} \left(\frac{d\phi_+}{dx} \right)^2 \right], \tag{18}$$

once we redefine the θ_+ field, $\theta_+ \to \theta_+ - \langle d\theta_+/dx \rangle x$, to absorb the nonvanishing average $\langle d\theta_+/dx \rangle$. Hence the ground state is a one-component TL liquid.

We are now ready to calculate correlation functions. Most important of these is the ground-state average of the vector chirality (5),

$$\langle \kappa_l^{(1)} \rangle = - b^2 \langle \sin(\sqrt{2\pi}\theta_-) \rangle = \mp b^2 c_1, \tag{19a}$$

$$\langle \kappa_l^{(2)} \rangle = - \sqrt{\frac{\pi}{2}} c_2 \left\langle \frac{d\theta_+}{dx} \right\rangle = \mp c_2(\pi - 2Q), \tag{19b}$$

where c_1 and c_2 are positive constants. These nonvanishing averages indicate that the ground state breaks a Z_2 symmetry and has a vector chiral long-range order. Since $\langle \kappa_l^{(1)} \rangle$ and $\langle \kappa_l^{(2)} \rangle$ have the same sign and satisfy Eq. (6), the spin current $J_n \langle \kappa_l^{(n)} \rangle$ flows as depicted in Fig. 3. The spin current circulates in each triangle in alternating fashion, and there is no net spin current flow through the whole system.

Two-point correlation functions are also calculated using Eqs. (11), (12), (17a), (17b), and (18). Here we remind the reader our convention that the site index l in the original lattice Hamiltonian (1) is equal to $2j+n$, where the integer j is the site index in each antiferromagnetic Heisenberg chain ($n=1,2$) in the two-chain (zigzag ladder) picture. Hence $\Delta l = 2\Delta j = 2\Delta x$. The correlation function for the vector chirality is given by

$$\langle \kappa_0^{(2)} \kappa_l^{(2)} \rangle = \langle \kappa^{(2)} \rangle^2 \left(1 - \frac{1}{K_+[(\pi - 2Q)l]^2} \right) + \frac{(-1)^l A_\kappa}{|l|^{4K_+}} \cos(2\pi M l) + \cdots, \tag{20}$$

where A_κ is a constant ($\propto b'^4 g_1^2$). In the two-point function of the chiral operator $\kappa_l^{(1)}$ the uniform $1/l^2$ term in Eq. (20) is replaced by a $1/l^4$ term.[30] The transverse- and longitudinal-spin-correlation functions are obtained as

$$\langle s_0^x s_l^x \rangle = \frac{A}{|l|^{1/4K_+}} \cos(Ql) + \cdots, \tag{21}$$

$$\langle s_0^z s_l^z \rangle = M^2 - \frac{K_+}{\pi^2 l^2} + \cdots. \tag{22}$$

Lastly the nematic correlation function shows a faster decay,

$$\langle s_0^+ s_1^+ s_l^- s_{l+1}^- \rangle = \frac{A'}{|l|^{1/K_+}} \cos(2Ql) + \cdots. \tag{23}$$

In the above equations A and A' are nonuniversal constants, and we have omitted subleading algebraically decaying terms and exponentially decaying terms, such as a short-ranged incommensurate correlation [$\propto \cos(\pi M l)$] in Eq. (22).

We note that the wave number of the transverse-spin-correlation function—the pitch angle—is shifted from the commensurate value $\pi/2$ to Q. The vector chiral long-range order and the incommensurate transverse-spin correlation are the hallmark of the vector chiral phase.

B. Numerical results

Here we present our numerical results, which support the theory of Sec. V A. The calculation was done for finite open

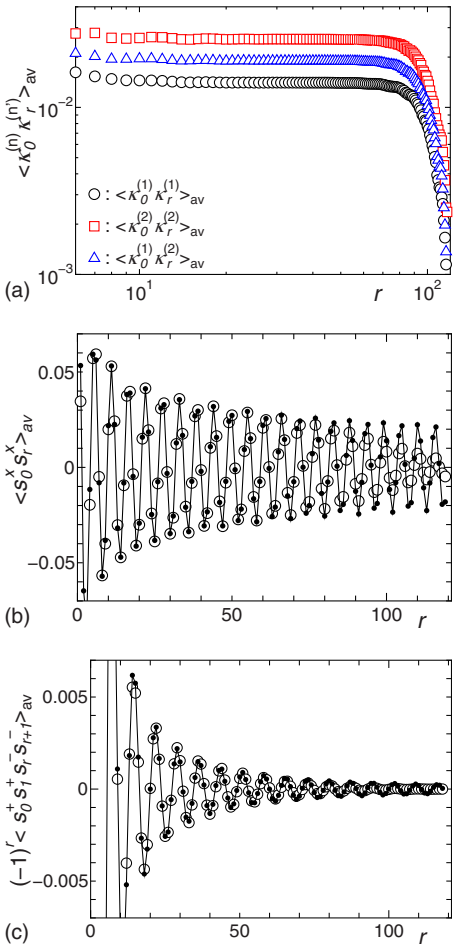

FIG. 10. (Color online) Averaged correlation functions for $L=120$ spins with $J_1/J_2=-2.7$ and $M=0.1$ in the vector chiral phase: (a) vector chiral correlation functions $\langle\kappa_0^{(1)}\kappa_r^{(1)}\rangle_{\rm av}$, $\langle\kappa_0^{(2)}\kappa_r^{(2)}\rangle_{\rm av}$, and $\langle\kappa_0^{(1)}\kappa_r^{(2)}\rangle_{\rm av}$, where $\kappa_r^{(n)}=(\boldsymbol{s}_r\times\boldsymbol{s}_{r+n})^z$ [Eq. (5)], (b) transverse-spin-correlation function $\langle s_0^x s_r^x\rangle_{\rm av}$, and (c) nematic correlation function $\langle s_0^+ s_1^+ s_r^- s_{r+1}^-\rangle_{\rm av}$. Open symbols represent the DMRG data. Truncation errors are smaller than the size of the symbols. The solid lines and solid circles in (b) and (c) are fits to Eqs. (21) and (23), respectively.

chains with $L=96$ and 120 sites, unless otherwise mentioned. In the following, we show mainly the results for $L=120$, while we note that the results for $L=96$ exhibit essentially the same behaviors as those for $L=120$. The number of kept DMRG states is up to 350. We have performed typically 10–30 DMRG sweeps in the calculation and checked the convergence of the results. Since Eqs. (19a), (19b), and (20)–(23) are obtained for infinite-length chains, we need to take care of open-boundary effects in the DMRG data to make meaningful comparison between the theory and the numerics. To reduce the boundary effects, we calculate two-point correlation functions for several pairs of two sites (l,l') with fixed distance $r=|l-l'|$ selecting the two sites being as close to the center of the chain as possible. We then take their average for the estimate of the correlation. We use the notation $\langle\cdots\rangle_{\rm av}$ for the averaged correlation functions below.

Figure 10(a) shows a typical r dependence of the averaged vector chiral correlation functions in the vector chiral phase ($J_1/J_2=-2.7$ and $M=0.1$). We clearly see that the vector chirality is long-range ordered.[50] We also find that not only $\langle\kappa_0^{(1)}\kappa_r^{(1)}\rangle_{\rm av}$ and $\langle\kappa_0^{(2)}\kappa_r^{(2)}\rangle_{\rm av}$ but also $\langle\kappa_0^{(1)}\kappa_r^{(2)}\rangle_{\rm av}$ are positive, in agreement with Eqs. (19a) and (19b). This indicates the ferrochiral order as drawn in Fig. 3.

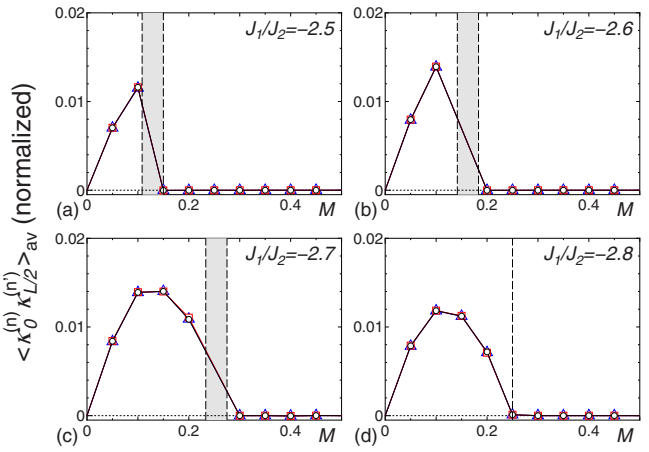

FIG. 11. (Color online) Averaged, normalized vector chiral correlations at the distance $r=L/2$ for $L=120$ spin zigzag chain. Circles, squares, and triangles represent $\langle\kappa_0^{(1)}\kappa_{L/2}^{(1)}\rangle$, $(2J_2/|J_1|)^2\langle\kappa_0^{(2)}\kappa_{L/2}^{(2)}\rangle$, and $(2J_2/|J_1|)\langle\kappa_0^{(1)}\kappa_{L/2}^{(2)}\rangle$, respectively. (a) $J_1/J_2=-2.5$, (b) $J_1/J_2=-2.6$, (c) $J_1/J_2=-2.7$, and (d) $J_1/J_2=-2.8$. Solid lines are the guide for the eyes. Vertical dashed lines represent the boundaries of the chiral ordered phase in low magnetization regime and the chiral disordered phase in the high magnetization regime. The shaded region corresponds to the magnetization jump at the first-order transition.

In Fig. 11 we plot averaged vector chiral correlations at a distance $r=L/2$ normalized by the coupling ratio, $\langle\kappa_0^{(1)}\kappa_{L/2}^{(1)}\rangle$, $(2J_2/|J_1|)\langle\kappa_0^{(1)}\kappa_{L/2}^{(2)}\rangle$, and $(2J_2/|J_1|)^2\langle\kappa_0^{(2)}\kappa_{L/2}^{(2)}\rangle$, as functions of M and J_1/J_2. The three quantities agree, as expected from Eq. (6). This figure clearly shows where the vector chiral correlation is strong; the vector chiral order exists in the low-field regime but disappears in the high-field regime. The shaded regions in Fig. 11 correspond to the magnetization jump discussed in Sec. IV, where the transition is clearly first order. We note that near the boundary of the vector chiral phase the vector chiral correlations suffer boundary effects in open chains and may underestimate the vector chiral order (see the discussion at the end of this section).

We fitted the DMRG data of the transverse-spin and nematic correlation functions to Eqs. (21) and (23), taking K_+, Q, and the amplitudes A or A' as fitting parameters. In the fitting procedure, we used the data of the averaged correlation function $\langle s_0^x s_r^x\rangle_{\rm av}$ $[\langle s_0^+ s_1^+ s_r^- s_{r+1}^-\rangle_{\rm av}]$ for $L/12\le r\le L/2$ $(L/6\le r\le L/2)$. Figures 10(b) and 10(c) demonstrate good agreement between numerical data and the fits to Eqs. (21) and (23). Note that both correlation functions are incommensurate.

The exponent K_+ and the incommensurate wave number Q obtained from the fitting are shown in Fig. 12. The TL-liquid parameter K_+ is found to be in the range $0.4<K_+<0.8$ for the cases we examined numerically, and the transverse-spin-correlation function $\langle s_0^x s_r^x\rangle_{\rm av}$ is the most slowly decaying correlation function except for the long-range ordered vector chirality. This suggests that a magnetic

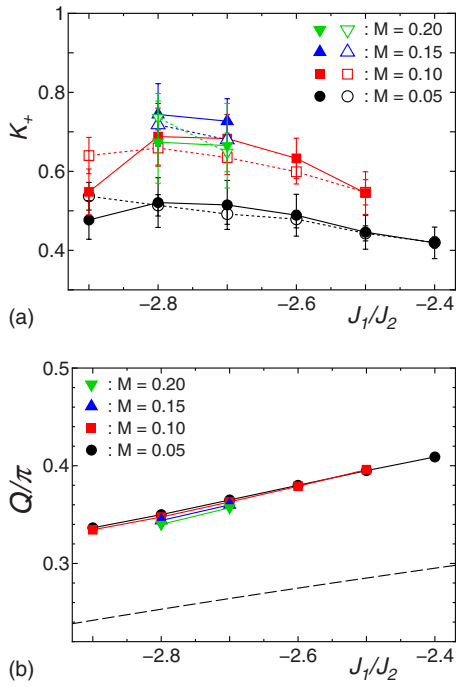

FIG. 12. (Color online) J_1/J_2 dependence of (a) the exponent K_+ and (b) the incommensurate wave number Q for $L=120$ spin zigzag chain in the vector chiral phase. Solid and open symbols in (a) represent the estimates obtained from the fitting of $\langle s_0^x s_r^x \rangle_{\rm av}$ and $\langle s_0^+ s_1^+ s_r^- s_{r+1}^- \rangle_{\rm av}$, respectively. The error bars represent the difference of the estimates obtained from the fitting of the data of different ranges. In (b), only the results from $\langle s_0^x s_r^x \rangle_{\rm av}$ are shown since the estimates from $\langle s_0^x s_r^x \rangle_{\rm av}$ and $\langle s_0^+ s_1^+ s_r^- s_{r+1}^- \rangle_{\rm av}$ are identical to each other within their error bars. Dashed line in (b) represents the classical pitch angle, $\phi^c = \arccos(-J_1/4J_2)$.

spiral long-range order in the plane perpendicular to the magnetic field should be realized in real three-dimensional materials with additional weak interchain couplings. The wave number Q, which represents the incommensurability of the transverse-spin correlations, shows little dependence on M and decreases as J_1/J_2 decreases. The classical analog of the wave number Q is the pitch angle $\phi^c = \arccos(-J_1/4J_2)$, which shows qualitatively the same feature, but takes a much smaller value. We have thus found that the incommensurate wave number is highly renormalized by quantum fluctuations toward the commensurate value $\pi/2$.

Strictly speaking, the bosonization theory of Sec. V A is not directly applicable when the interchain ferromagnetic coupling is strong, $|J_1|/J_2 \gtrsim 1$. The consistency between the theory and numerics, as demonstrated by the successful fitting, can be understood once we postulate that the vector chiral phase extends to the limit $J_1/J_2 \to 0$, where the bosonization approach is valid, and that the low-energy physics in this phase is governed by the same effective theory.

In passing we note that for $J_1/J_2 \lesssim -2.9$ we have not found clear evidence for long-range order of vector chirality; although the vector chiral correlation is strong, it seems to decay slowly at long distances in finite-size systems $L \leq 120$. A possible explanation for this behavior would be that the energy gap in the antisymmetric sector (ϕ_-, θ_-) is so small that the correlation length becomes very large. As a result, the bending-down behavior of the vector chiral correlation functions,[50] observed near the open boundaries ($r \sim L$) in Fig. 10(a), penetrates into the bulk region and spoils long-range order. For clarifying the fate of the vector chiral order for $J_1/J_2 \lesssim -2.9$, calculations for much larger systems are needed. That is left for future studies.

VI. NEMATIC PHASE AND SPIN-DENSITY-WAVE PHASE

In this section we discuss in detail the nematic phase and the SDW_2 phase, where two magnons form a bound state with total momentum $k=\pi$. As we saw in Sec. IV the total magnetization changes in units of $\Delta S^z_{\rm tot}=2$ as a result of simultaneous flip of two spins forming a bound state. We first review the application of the bosonization theory described in Sec. V A to these phases for the sake of completeness of our discussion which partly complements earlier works.[3,7,29] We then present an alternative phenomenological theory[6] in which a bound magnon pair is regarded as a hard-core boson. The theoretical picture developed in these discussions is subsequently confirmed by numerics.

A. Bosonization theory revisited

The nematic phase can be described within the bosonization approach for $|J_1| \ll J_2$. When the g_1 coupling in the effective Hamiltonian (13) is the most relevant, the field ϕ_- is pinned at a value which minimizes the g_1 term,

$$\langle \phi_-(x) \rangle = \sqrt{\frac{\pi}{8}} \left(\frac{1}{2} - M \right). \tag{24}$$

In this case the uniform part of the difference of two neighboring spins vanishes, $s^z_l - s^z_{l+1} \sim \sqrt{2/\pi}\partial_x \phi_- = 0$, indicating that two spins are bound.[2,3,7,29] The dual field θ_- is strongly fluctuating and the g_2 is irrelevant. The fields ϕ_+ and θ_+ of the symmetric sector remain gapless and constitute a one-component TL liquid (18).

The long-distance asymptotic form of correlation functions can be readily obtained from Eqs. (11), (12), (18), and (24). We briefly summarize the results below.

The longitudinal-spin correlation has an incommensurate oscillatory component,

$$\langle s^z_0 s^z_l \rangle = M^2 - \frac{K_+}{\pi^2 l^2} + \frac{B}{|l|^{K_+}} \cos\left[\pi l \left(\frac{1}{2} - M \right) \right] + \cdots, \tag{25}$$

where B is a positive constant ($\propto a^2$) and subleading terms are omitted here and in the equations below. The third term in Eq. (25) represents incommensurate spin-density-wave correlation.

The transverse-spin correlation $\langle s^+_0 s^-_l \rangle$ is short ranged, whose correlation length is the inverse of the gap in the (ϕ_-, θ_-) sector. Physically, this gap corresponds to the binding energy of the two-magnon bound state.

The composite operator $s^-_l s^-_{l+1}$ creating a two-magnon bound state represents the nematic order. The nematic correlation is alternating and quasi-long-ranged,

$$\langle s_0^+ s_1^+ s_l^- s_{l+1}^- \rangle = \frac{B'(-1)^l}{|l|^{1/K_+}} - \frac{B''(-1)^l}{|l|^{K_+ + 1/K_+}} \cos\left[\pi l\left(\frac{1}{2} - M\right)\right] + \cdots \tag{26}$$

with B' and B'' as positive constants. Here we note that two down spins are created and annihilated at neighboring sites in Eq. (26). In fact, the algebraic decay with the same exponent can be obtained as long as both distances between the created down spins and between the annihilated ones are odd integers. However, when these separations are even, the nematic correlation functions, $\langle s_0^+ s_{2n}^+ s_l^- s_{l+2n'}^- \rangle$ $(n, n' \ll l)$, are expected to be weaker, as they involve the gapped θ_- field in lowest order. This is in accordance with the observation we made in Sec. III that the wave function of the two-magnon bound state with $k=\pi$ at a saturation field is a linear combination of the states in which the distance between two down spins is restricted to odd integers.

Comparing Eqs. (25) and (26), we find that the nematic correlation (26) is the most dominant correlation if $K_+ > 1$. This phase is called nematic phase. On the other hand, if $K_+ < 1$, the most dominant correlation is the longitudinal-spin correlation (25). In this case we have the SDW_2 phase.

The vector chiral correlation $\kappa^{(2)}$ shows a power-law decay,

$$\langle \kappa_0^{(2)} \kappa_l^{(2)} \rangle = -\frac{c_2^2}{K_+ l^2} + \cdots . \tag{27}$$

The same $1/l^2$ decay (with a different prefactor) is expected for $\langle \kappa_0^{(1)} \kappa_l^{(1)} \rangle$, as the operator product of $\sin(\sqrt{2\pi}\theta_-)$ and the irrelevant g_2 term in the Hamiltonian $\tilde{\mathcal{H}}$ generates the $d\theta_+/dx$ operator.

In his pioneering paper, Chubukov[1] suggested that the nematic phase should have spontaneous dimerization, $\langle s_l^z (s_{l+1}^z - s_{l-1}^z) \rangle \propto (-1)^l$. However, in the bosonization theory the dimerization operator is proportional to $\cos(\sqrt{8\pi}\phi_- + \pi M)$, whose average vanishes because of Eq. (24). We thus conclude that the nematic phase does not have a spontaneous dimerization.

B. Hard-core Bose gas of bound magnons

As we discussed in Sec. III, when $-2.7 \lesssim J_1/J_2 < 0$, the fully polarized state becomes unstable as a result of formation of two-magnon bound states at the saturation field h_s.[1–3,6,7] Below h_s, bound magnon pairs collectively form a TL liquid with nematic correlation as well as incommensurate longitudinal-spin correlation. Here we develop a phenomenological theory for the phases which emerge as a result of proliferation of p-magnon bound states with momentum $k=\pi$ by assuming that tightly bound p magnons can be treated as a hard-core boson[51] and ignoring internal structure of the bound states. This is expected to be a good approximation as long as the density of hard-core bosons is very low, i.e., near the saturation field. As we will see below, for the $p=2$ case, this theory is equivalent to the (ϕ_+, θ_+) sector of the bosonization theory.

We denote creation and annihilation operators of a hard-core boson by $b_l^\dagger$ and b_l. Under the assumption that p magnons are tightly bound, we may relate the creation operator and density operator of bosons to spin operators,

$$b_l^\dagger = (-1)^l s_l^- \cdots s_{l+p-1}^-, \tag{28}$$

$$b_l^\dagger b_l = \frac{1}{p}\left(\frac{1}{2} - s_l^z\right), \tag{29}$$

where the $(-1)^l$ factor in Eq. (28) is introduced because the total momentum of bound p magnons is $k=\pi$ (see Sec. III). In Eq. (28) we identify the site index $\bar{l}$ of the boson creation operator $b_{\bar{l}}^\dagger$ with the center-of-mass coordinate of bound magnons, $\bar{l} = l + (p-1)/2$. From Eq. (29) we find the density of bosons,

$$\rho = \frac{1}{p}\left(\frac{1}{2} - M\right). \tag{30}$$

At small but finite density $0 < \rho \ll 1$ the hard-core bosons are a TL liquid at low energy.[52] Its low-energy effective theory is again a free field theory,

$$\mathcal{H}_0 = \frac{v}{2}\int_{-\infty}^{\infty} d\bar{x}\left[K\left(\frac{d\theta}{d\bar{x}}\right)^2 + \frac{1}{K}\left(\frac{d\phi}{d\bar{x}}\right)^2\right], \tag{31}$$

where the bosonic fields (ϕ, θ) play the same role as the (ϕ_+, θ_+) fields in the $p=2$ case. Here, we take the lattice spacing between lth and $(l+1)$th sites to be unity and identify l (or $\bar{l}$) with $\bar{x}$. The TL-liquid parameter K depends on interactions that work between bosons in addition to the short-range hard-core repulsion. When hard-core bosons are free, $K=1$. This should be the case in the low-density limit $M \to \frac{1}{2}^-$. In the continuum limit the operators $b_l^\dagger$ and $b_l^\dagger b_l$ are written as[52]

$$b_l^\dagger = \sqrt{\rho} e^{i\sqrt{\pi}\theta} \sum_{n=-\infty}^{\infty} e^{2in(\pi\rho\bar{x} + \sqrt{\pi}\phi)}, \tag{32}$$

$$b_l^\dagger b_l = \rho + \frac{1}{\sqrt{\pi}}\frac{d\phi}{d\bar{x}} + \rho\cos(2\pi\rho\bar{x} + \sqrt{4\pi}\phi) + \cdots . \tag{33}$$

Using these bosonization formulas, it is straightforward to calculate correlation functions of hard-core bosons. Equations (28) and (29) allow us to express these correlation functions with the original spins $\boldsymbol{s}_l$; we thus obtain the longitudinal-spin and p-magnon (multipolar) correlation functions, $\langle s_l^z s_{l'}^z \rangle$ and $\langle s_l^+ \cdots s_{l+p-1}^+ s_{l'}^- \cdots s_{l'+p-1}^- \rangle$, from the density-density correlation function and the propagator of the bosons, respectively. In the thermodynamic limit $L \to \infty$ we find

$$\langle s_0^z s_l^z \rangle = \left\langle \left(\frac{1}{2} - p b_0^\dagger b_0\right)\left(\frac{1}{2} - p b_l^\dagger b_l\right) \right\rangle = M^2 - \frac{p^2 \eta}{4\pi^2 l^2} + \frac{A_z \cos(2\pi\rho l)}{|l|^\eta} + \cdots , \tag{34}$$

$$\langle s_0^+ \cdots s_{p-1}^+ s_l^- \cdots s_{l+p-1}^- \rangle = (-1)^l \langle b_0^\dagger b_l^\dagger \rangle = \frac{A_m(-1)^l}{|l|^{1/\eta}} - \frac{\tilde{A}_m(-1)^l}{|l|^{\eta+1/\eta}} \cos(2\pi\rho l) + \cdots, \tag{35}$$

where A_z, A_m, and $\tilde{A}_m$ are positive constants and the parameter η in the exponents is related to the TL-liquid parameter K by $\eta=2K$. Since creating less than p magnons costs a finite energy, we expect that the transverse-spin-correlation functions $\langle s_l^x s_{l'}^x \rangle$ and, more generally, $\langle s_l^+ \cdots s_{l+p'-1}^+ s_{l'}^- \cdots s_{l'+p'-1}^- \rangle$ with $p' < p$ should be short ranged.

When $p=2$, Eqs. (34) and (35) coincide with Eqs. (25) and (26) by using relation (30) and setting the exponent $\eta = K_+$. That is, the two theoretical approaches, the weak-coupling bosonization theory[7] for $|J_1| \ll J_2$ and the phenomenological hard-core boson theory[6] for $\frac{1}{2} - M \ll 1$, give a consistent description of the nematic and SDW_2 phases. This is in fact expected, as the nematic TL liquid extends from the saturation limit ($M \to \frac{1}{2}$) to the weak interchain coupling regime $|J_1| \ll J_2$ (see Fig. 1).

To compare the above theoretical results with numerical data from DMRG calculation, we need to modify Eqs. (34) and (35) to include finite-size and boundary effects. This can be done by calculating the correlation functions with Dirichlet boundary conditions on $\phi(\bar{x})$. Here we can borrow results of such calculations from Refs. 45 and 46, in which correlation functions of the spin-1/2 *XXZ* model in magnetic field are obtained for open spin chains of length L, once we notice the mapping of the hard-core boson system onto the spin-1/2 *XXZ* chain [$S_l^- = (-1)^l b_l$ and $S_l^z = b_l^\dagger b_l - \frac{1}{2}$]. In this way we obtain local spin polarization $\langle s_l^z \rangle$ in the J_1-J_2 spin chain of length L,

$$\langle s_l^z \rangle = \frac{1}{2}(1-p) - p z(l;q), \tag{36}$$

where

$$z(l;q) = \frac{q}{2\pi} - a\frac{(-1)^l \sin(ql)}{f_{\eta/2}(2l)}, \tag{37}$$

$$q = \frac{2\pi L}{L+1}\left(\rho - \frac{1}{2}\right), \tag{38}$$

$$f_\nu(x) = \left[\frac{2(L+1)}{\pi}\sin\left(\frac{\pi|x|}{2(L+1)}\right)\right]^\nu. \tag{39}$$

The site dependence of the polarization $\langle s_l^z \rangle$ comes from Friedel oscillations at open boundaries. Such oscillations are absent under periodic boundary conditions. The characteristic wave vector $2k_F$ in the Friedel oscillations is found from Eqs. (36)–(38) for $L \gg 1$ to be

$$2k_F = 2\pi\rho, \tag{40}$$

which is determined by the density of the hard-core bosons, and is inversely proportional to the number p of magnons forming a bound state [see relation (30)]. This result can be easily checked by DMRG calculation.

The longitudinal-spin-correlation function in the finite J_1-J_2 spin chain is given by

$$\langle s_l^z s_{l'}^z \rangle = \frac{(p-1)^2}{4} + \frac{p(p-1)}{2}[z(l;q) + z(l';q)] + p^2 Z(l,l';q), \tag{41}$$

where

$$\begin{aligned} Z(l,l';q) = {} & \left(\frac{q}{2\pi}\right)^2 - \frac{\eta}{4\pi^2}\left[\frac{1}{f_2(l-l')} + \frac{1}{f_2(l+l')}\right] \\ & - \frac{aq}{2\pi}\left[\frac{(-1)^l \sin(ql)}{f_{\eta/2}(2l)} + \frac{(-1)^{l'} \sin(ql')}{f_{\eta/2}(2l')}\right] \\ & + \frac{(-1)^{l-l'} a^2}{2 f_{\eta/2}(2l) f_{\eta/2}(2l')}\left\{\cos[q(l-l')]\frac{f_\eta(l+l')}{f_\eta(l-l')}\right. \\ & \left. - \cos[q(l+l')]\frac{f_\eta(l-l')}{f_\eta(l+l')}\right\} \\ & - \frac{a\eta}{2\pi}\left\{\frac{(-1)^l \cos(ql)}{f_{\eta/2}(2l)}[g(l+l') + g(l-l')]\right. \\ & \left. + \frac{(-1)^{l'} \cos(ql')}{f_{\eta/2}(2l')}[g(l+l') - g(l-l')]\right\} \end{aligned} \tag{42}$$

with

$$g(x) = \frac{\pi}{2(L+1)}\cot\left[\frac{\pi x}{2(L+1)}\right]. \tag{43}$$

From Eqs. (36) and (41), the correlation of longitudinal-spin fluctuations is obtained as

$$\langle s_l^z s_{l'}^z \rangle - \langle s_l^z \rangle \langle s_{l'}^z \rangle = p^2[Z(l,l';q) - z(l;q)z(l';q)]. \tag{44}$$

We have two unknown parameters, a and η, in these formulas, which can be obtained by fitting numerical data to these analytical forms.

Similarly, the multipolar correlation is obtained as

$$\langle s_l^+ \cdots s_{l+p-1}^+ s_{l'}^- \cdots s_{l'+p-1}^- \rangle = A_m(-1)^{l-l'} \frac{f_{1/2\eta}(2l+p-1) f_{1/2\eta}(2l'+p-1)}{f_{1/\eta}(l-l') f_{1/\eta}(l+l'+p-1)}, \tag{45}$$

which corresponds to the first term in the right-hand side of Eq. (35). Here fitting parameters are A_m and η.

Before closing this section, we note once again that the phenomenological hard-core boson theory is applicable to any phase which appears as a result of the formation of p-magnon bound states with $p=2,3,4,\cdots$ and $k=\pi$. We will show in Secs. VI C and VIII that the phenomenological theory gives a good description of correlation functions not only in the nematic and SDW_2 ($p=2$) phases but also in the triatic and SDW_3 ($p=3$) phases and quartic ($p=4$) phase, which appear for larger $|J_1|/J_2$. Another advantage of the theory is that it gives a clear intuitive picture of low-energy

excitations. It is however unable to describe correlations that are related to internal structures of bound states [such as the feature we discussed below Eq. (26)].

C. Numerical results

We apply the phenomenological hard-core boson theory to analyze numerical results in this section. We use the DMRG method to compute the longitudinal- and transverse-spin correlations, the nematic correlation function, and the local spin polarization in finite open chains. We fit the correlation functions to Eqs. (36)–(45) with $p=2$, taking the exponent η and the coefficients a and A_m as fitting parameters. Since the formulas already include effects of open boundaries, here we do not have to take spatial average of the correlation functions in the fitting procedure. Finite-size effects are also properly taken into account in these formulas. Indeed, we have observed that fitting of numerical results for $L=96$ and $L=120$ yields the same good quality of agreement between the numerical data and the fits and gives essentially the same estimated values of the fitting parameters. The results for $L=120$ are shown below.

Figures 13(a) and 13(b) show DMRG results of $\langle s_l^z\rangle$ and $\langle s_l^z s_{l'}^z\rangle - \langle s_l^z\rangle\langle s_{l'}^z\rangle$ calculated for $J_1/J_2=-2.0$ at $M=0.2$ and 0.4. Shown in the same figures are the fits to Eqs. (36) and (44), respectively, with $p=2$. We have used numerical data for $6 \le l \le L-5$ to fit $\langle s_l^z\rangle$ and data for $11 \le |l-l'| \le L-10$ to fit $\langle s_l^z s_{l'}^z\rangle - \langle s_l^z\rangle\langle s_{l'}^z\rangle$ and obtained excellent agreement for both. (Note that there are only two free parameters η and a in the fitting.) The data of $\langle s_l^z\rangle$ show Friedel oscillations whose wavelength is in good agreement with the theoretical prediction with $p=2$ (without any fitting parameter). This is another evidence of the formation of bound magnon pairs. We observed this consistency in the whole region of the nematic and SDW_2 phases. The results clearly indicate that the low-energy physics in this parameter range is indeed described by the effective theory of hard-core bosons of bound magnon pairs.

For the nematic correlation $\langle s_l^+ s_{l+1}^+ s_{l'}^- s_{l'+1}^-\rangle$, we fit the DMRG result to Eq. (45) with $p=2$, ignoring the additional oscillating component seen in the DMRG data which would correspond to the subleading term in Eq. (45). We see in Fig. 13(c) that the leading power-law decaying behavior of $(-1)^{l-l'}\langle s_l^+ s_{l+1}^+ s_{l'}^- s_{l'+1}^-\rangle$ is fitted rather well by Eq. (45). Figure 13(d) shows that the transverse-spin-correlation function decays exponentially, as expected from a finite-energy cost for breaking a two-magnon bound state. These results also support the validity of the effective theory of hard-core Bose gas of bound magnon pairs.

Figure 14 shows the estimate of η obtained from the fitting of $\langle s_l^z s_{l'}^z\rangle$. As M increases, the exponent η increases across the dashed line $\eta=1$. Therefore, the ground state undergoes a crossover from the low-field SDW_2 phase, where the longitudinal-spin-correlation function is dominant, to the high-field nematic phase, where the nematic correlation dominates.[7] We have found that η estimated from the other correlators, $\langle s_l^z\rangle$, $\langle s_l^z s_{l'}^z\rangle - \langle s_l^z\rangle\langle s_{l'}^z\rangle$, and $\langle s_l^+ s_{l+1}^+ s_{l'}^- s_{l'+1}^-\rangle$, are consistent with Fig. 14. As $M \to \frac{1}{2}^-$, η increases toward $\eta=2$, in

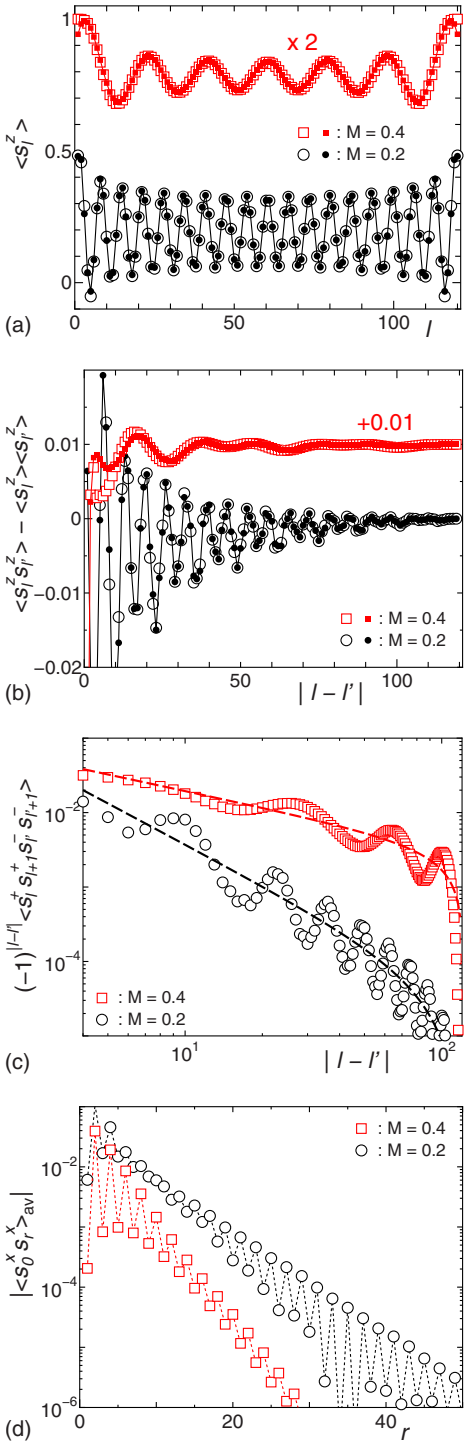

FIG. 13. (Color online) Correlation functions for $L=120$ spin zigzag chain with $J_1/J_2=-2.0$, $M=0.2$ and 0.4, and their fits to the theory for the nematic and SDW_2 phases: (a) Friedel oscillations in the local spin polarization $\langle s_l^z\rangle$, (b) longitudinal-spin fluctuation $\langle s_l^z s_{l'}^z\rangle - \langle s_l^z\rangle\langle s_{l'}^z\rangle$, and (c) nematic correlation function $\langle s_l^+ s_{l+1}^+ s_{l'}^- s_{l'+1}^-\rangle$. The open symbols represent the DMRG data. Truncation errors are smaller than the size of the symbols. In (b) and (c), the data for $l = L/2-[r/2]$ and $l' = L/2+[(r+1)/2]$ are plotted as a function of $r=|l-l'|$. The results of the fitting are shown by solid symbols in (a) and (b) and by dashed curves in (c). The data for $M=0.4$ are multiplied by a factor 2 in (a) and shifted by 0.01 in (b). (d) Absolute values of the averaged transverse-spin-correlation function $\langle s_0^x s_r^x\rangle_{\rm av}$.

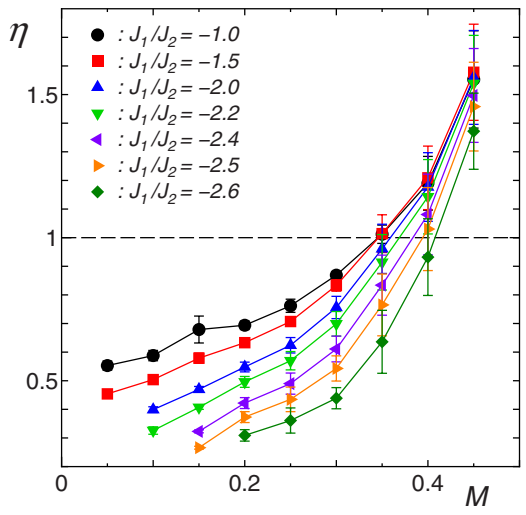

FIG. 14. (Color online) M dependence of the exponent η in the nematic phase ($\eta>1$) and SDW$_2$ phase ($\eta<1$). The estimates are obtained from the fitting of $\langle s_l^z s_{l'}^z\rangle$. The error bars represent the difference of the estimates obtained from the fitting using the data of different ranges.

agreement with the theoretical prediction that the hard-core bosons become free in the dilute limit.

VII. INCOMMENSURATE NEMATIC PHASE

As we discussed in Sec. III, for $-2.720<J_1/J_2<-2.669$ the fully polarized state becomes unstable at the saturation field as a result of formation of two-magnon bound states with an incommensurate momentum.[6] Below the saturation field these bound states are expected to form a TL liquid with incommensurate nematic correlation. Such an incommensurate nematic phase was predicted by Chubukov,[1] who dubbed this phase the chiral biaxial spin nematic, as he considered it to have long-range vector chiral order. However, our numerical results indicate that the vector chirality is not long ranged in the incommensurate nematic phase.

Figure 15 shows our DMRG results of spatially averaged correlation functions for $J_1/J_2=-2.7$ and $M=0.4$. We see in Figs. 15(a) and 15(b) that the correlation of the longitudinal-spin fluctuations $[\langle s_0^z s_r^z\rangle-\langle s_0^z\rangle\langle s_r^z\rangle]_{\rm av}$ and the nematic correlation function $\langle s_0^+ s_1^+ s_r^- s_{r+1}^-\rangle_{\rm av}$ decay slowly (presumably algebraically) with an incommensurate modulation. On the other hand, we find in Fig. 15(c) that the transverse-spin correlation $\langle s_0^x s_r^x\rangle_{\rm av}$ decays exponentially, indicating the existence of a finite binding energy of the two-magnon bound pairs. Finally, Fig. 15(d) shows that the correlation functions of vector chirality $\kappa_l^{(n)}$ have at most quasi-long-range order with incommensurate oscillations.

In Fig. 16, we show the local spin polarization $\langle s_l^z\rangle$ and its Fourier transform for $L=80$, 120, and 160. The Fourier transform exhibits three peaks. This is in contrast to the cases of the nematic phase in Sec. VI and the triatic and quartic phases (see Sec. VIII), where the polarization $\langle s_l^z\rangle$ is described by Eq. (36) with a single wave number q. The positions of peaks in the Fourier transform are almost indepen-

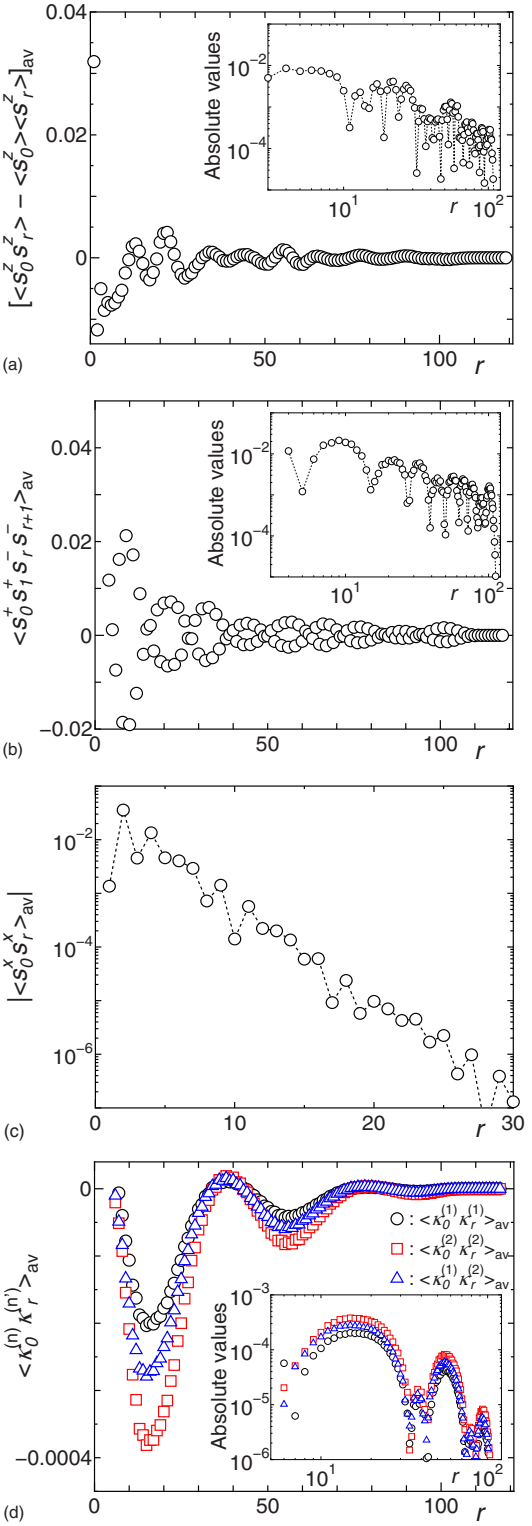

FIG. 15. (Color online) Averaged correlation functions for $L=120$ spin zigzag chain with $J_1/J_2=-2.7$ and $M=0.4$ in the incommensurate nematic phase: (a) longitudinal-spin fluctuation $[\langle s_0^z s_r^z\rangle-\langle s_0^z\rangle\langle s_r^z\rangle]_{\rm av}$, (b) nematic correlation function $\langle s_0^+ s_1^+ s_r^- s_{r+1}^-\rangle_{\rm av}$, (c) absolute values of the transverse-spin-correlation function $\langle s_0^x s_r^x\rangle_{\rm av}$, and (d) vector chiral correlation functions $\langle \kappa_0^{(1)}\kappa_r^{(1)}\rangle_{\rm av}$, $\langle \kappa_0^{(2)}\kappa_r^{(2)}\rangle_{\rm av}$, and $\langle \kappa_0^{(1)}\kappa_r^{(2)}\rangle_{\rm av}$. Truncation errors are smaller than the size of the symbols. Insets in (a), (b), and (d) show the absolute values of the data in a log-log scale.

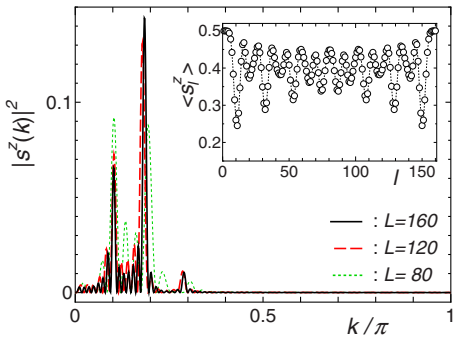

FIG. 16. (Color online) Squared modulus of the Fourier transform, $|s^z(k)|^2$, which is an even function of k and where $s^z(k) = (1/\sqrt{L})\Sigma_l e^{ikl}(\langle s_l^z \rangle - M)$, for $J_1/J_2 = -2.7$ and $M = 0.4$ in the incommensurate nematic phase. The solid, dashed, and dotted lines represents the data for $L = 160$, 120, and 80, respectively. Inset: the local spin polarization $\langle s_l^z \rangle$ for $J_1/J_2 = -2.7$, $M = 0.4$, and $L = 160$.

dent of L, suggesting that the incommensurability should not be due to finite-size nor open-boundary effects.

We have observed qualitatively the same behaviors of the correlation functions and spin polarization for $J_1/J_2 = -2.7$ and $M > M_c \approx 0.35$. From these results, we conclude that the incommensurate nematic phase (without chiral long-range order) exists in the narrow region of the phase diagram (see Fig. 1).

Unfortunately, we are not aware of an effective theory which can give consistent description of these numerical results. However, in the spirit of the hard-core boson theory in Sec. VI, we may try to treat the two-magnon bound states as hard-core bosons,

$$s_l^- s_{l+1}^- = e^{i(\pi+\delta)l} b_{1,\bar{l}}^\dagger + e^{i(\pi-\delta)\bar{l}} b_{2,\bar{l}}^\dagger, \tag{46}$$

$$\frac{1}{2}\left(\frac{1}{2} - s_l^z\right) = b_{1,l}^\dagger b_{1,l} + b_{2,l}^\dagger b_{2,l}, \tag{47}$$

where $b_{1,l}^\dagger$ and $b_{2,l}^\dagger$ are creation operators of hard-core bosons with momentum $k = \pi + \delta$ and $\pi - \delta$, respectively. The long-range order of vector chirality would follow if the average of the boson number difference, $b_1^\dagger b_1 - b_2^\dagger b_2$, became nonvanishing spontaneously. Figure 15(d) indicates that this is not the case and implies that the low-energy properties in this phase are determined by two bosonic modes ($b_1^\dagger b_1 + b_2^\dagger b_2$ and $b_1^\dagger b_1 - b_2^\dagger b_2$), forming a two-flavor TL liquid.

VIII. TRIATIC AND QUARTIC PHASES

In this section we consider the triatic, SDW_3, and quartic phases, in which the total magnetization changes by $\Delta S_{\rm tot}^z = 3$ and 4. We again apply the hard-core boson theory of Sec. VI B with $p = 3$ and 4.

Figure 17 shows our DMRG results for the triatic and SDW_3 phases. As a typical example, we chose the coupling ratio $J_1/J_2 = -3.0$ and magnetization per spin $M = 0.2$ and 0.4. We fit the local spin polarization $\langle s_l^z \rangle$ and the longitudinal-spin-fluctuation correlation $\langle s_l^z s_{l'}^z \rangle - \langle s_l^z \rangle \langle s_{l'}^z \rangle$ to Eqs. (36) and (44) with $p = 3$, respectively, taking η and a as fitting param-

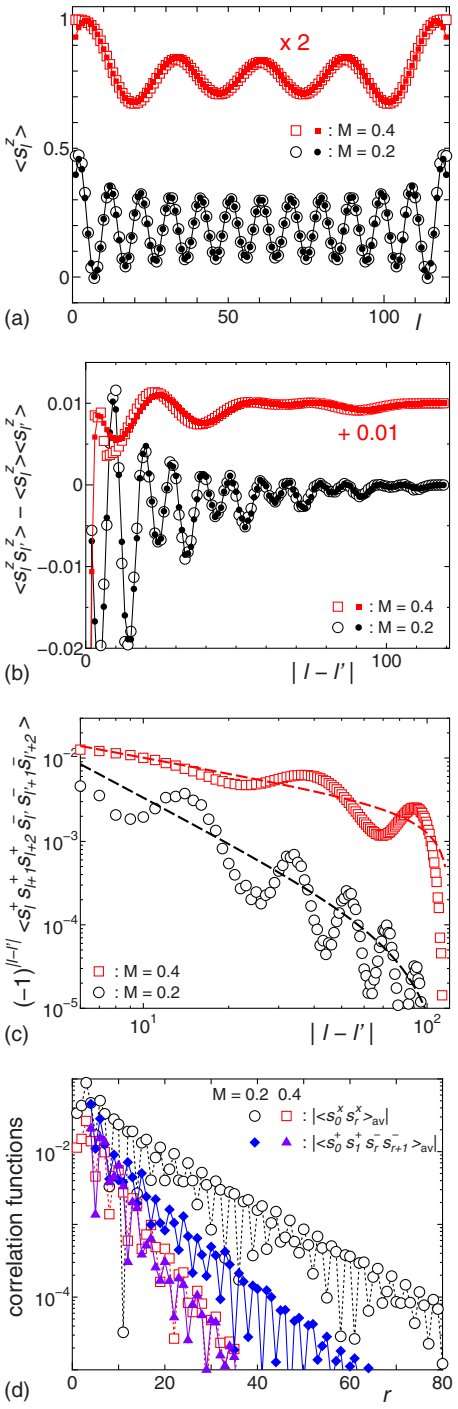

FIG. 17. (Color online) Correlation functions for $L = 120$ spin zigzag chain with $J_1/J_2 = -3.0$, $M = 0.2$ and 0.4 and their fits to the theory for the triatic phase: (a) Friedel oscillations in the local spin polarization $\langle s_l^z \rangle$, (b) longitudinal-spin fluctuation $\langle s_l^z s_{l'}^z \rangle - \langle s_l^z \rangle \langle s_{l'}^z \rangle$, and (c) triatic correlation function $\langle s_l^+ s_{l+1}^+ s_{l+2}^+ s_{l'}^- s_{l'+1}^- s_{l'+2}^- \rangle$. The open symbols represent the DMRG data. Truncation errors are smaller than the size of the symbols. In (b) and (c), the data for $l = L/2 - [r/2]$ and $l' = L/2 + [(r+1)/2]$ are plotted as a function of $r = |l - l'|$. The results of the fitting are shown by solid symbols in (a) and (b) and by dashed curves in (c). The data for $M = 0.4$ are multiplied by a factor 2 in (a) and shifted by 0.01 in (b). (d) Absolute values of the averaged transverse-spin and nematic correlation functions, $\langle s_0^x s_r^x \rangle_{\rm av}$ and $\langle s_0^+ s_1^+ s_r^- s_{r+1}^- \rangle_{\rm av}$.

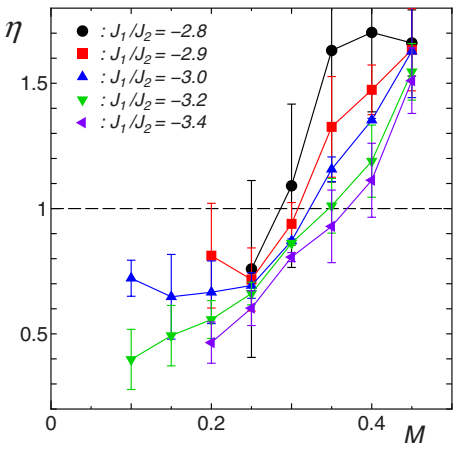

FIG. 18. (Color online) M dependence of the exponent η in the triatic phase ($\eta>1$) and SDW$_3$ phase ($\eta<1$). The estimates are obtained from the fitting of $\langle s_l^z s_{l'}^z\rangle$ for $J_1/J_2\geq -3.0$ and $\langle s_l^z\rangle$ for $J_1/J_2=-3.2$ and -3.4. The error bars represent the difference of the estimates obtained from the fitting using the data of different ranges.

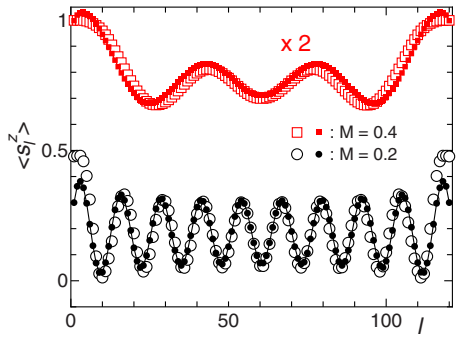

FIG. 19. (Color online) Friedel oscillations in the local spin polarization $\langle s_l^z\rangle$ for $L=120$ spin zigzag chain with $J_1/J_2=-3.6$ and $M=0.2$ and 0.4, and their fits to the theory for the quartic phase. The open symbols represent the DMRG data and solid symbols show the results of the fitting. Truncation errors of the DMRG data are smaller than the size of the symbols. The data for $M=0.4$ are multiplied by a factor 2.

eters. We find that these correlators are fitted quite well by the formulas. The fitting of the triatic correlation function $\langle s_l^+ s_{l+1}^+ s_{l+2}^+ s_{l'}^- s_{l'+1}^- s_{l'+2}^-\rangle$ to Eq. (45) with $p=3$ also works well within the approximation that the subleading oscillating terms are ignored. The transverse-spin and two-magnon (nematic) correlation functions, $\langle s_l^x s_{l'}^x\rangle$ and $\langle s_l^+ s_{l+1}^+ s_{l'}^- s_{l'+1}^-\rangle$, decay exponentially in accordance with the theoretical prediction. All these observations demonstrate the validity of the bosonic effective theory for the triatic/SDW$_3$ phases.

Figure 18 shows the exponent η obtained from the fitting of $\langle s_l^z s_{l'}^z\rangle$ for $J_1/J_2\geq -3.0$ and $\langle s_l^z\rangle$ for $J_1/J_2\leq -3.2$. Although the estimates have rather large error bars, there is a clear tendency that η increases from $\eta<1$ to $\eta>1$ as M increases. The estimates of η obtained from the other correlators, including the triatic correlation $\langle s_l^+ s_{l+1}^+ s_{l+2}^+ s_{l'}^- s_{l'+1}^- s_{l'+2}^-\rangle$ for $J_1/J_2\geq -3.0$, exhibit essentially the same feature. The result indicates that the ground state undergoes a crossover from the low-field SDW$_3$ phase with the dominant longitudinal-spin correlation to the high-field triatic phase where the three-magnon (triatic) correlation is dominant. The behavior of η at large M is also consistent with the theoretical prediction that $\eta\to 2$ as $M\to\frac{1}{2}^-$.

For the quartic phase, we show the local spin polarization $\langle s_l^z\rangle$ calculated at $J_1/J_2=-3.6$ and $M=0.2$ and 0.4. (The numerical data of other correlation functions are not available for $J_1/J_2<-3$ because of slow convergence of DMRG calculation.[53]) We clearly see in Fig. 19 that the numerical data of $\langle s_l^z\rangle$ are fitted well by Eq. (36) with $p=4$. This gives strong support for the presence of the quartic phase for these parameters from the following reason. As we emphasize below Eq. (40), the period of the Friedel oscillations in $\langle s_l^z\rangle$ is directly related to the density ρ of hard-core bosons and, in particular, the number p of magnons forming a bound state. Indeed, if we compare Figs. 13(a), 17(a), and 19 for the same magnetization M, we find that the number of nodes in $\langle s_l^z\rangle$ changes as $\propto 1/p$ for the nematic/SDW$_2$, triatic/SDW$_3$, and quartic phases. Therefore, the successful fitting of $\langle s_l^z\rangle$ to Eq. (36) with a certain p can be considered as a strong evidence for the formation of p-magnon bound states.

One may naturally expect that for the quartic phase a spin-density-wave (SDW$_4$) regime with dominant longitudinal-spin correlation should also appear at low magnetic field. Indeed, the exponent η obtained from the fitting of $\langle s_l^z\rangle$ for $J_1/J_2=-3.6$ (not shown here) exhibits a tendency that η changes from $\eta<1$ to $\eta>1$ with increasing M. Meanwhile, the estimates of η have large error bars, which prevent us from determining accurately the crossover point between the quartic and SDW$_4$ regions unfortunately. We therefore tentatively call the region of $\Delta S_{\rm tot}^z=4$ the quartic phase, keeping it in mind that the low-field part of the phase probably includes the SDW$_4$ regime.

IX. CONCLUDING REMARKS

We have determined the magnetic phase diagram of the spin-1/2 J_1-J_2 zigzag spin chain with ferromagnetic J_1 and competing antiferromagnetic J_2 interactions under magnetic field. Asymptotic behaviors of correlation functions have been derived for various phases using bosonization approach for weak J_1 and the effective theory for hard-core bosons of bound multimagnons. By fitting numerical data of the correlation functions obtained by the DMRG method to the analytic forms, we have successfully identified the vector chiral phase, nematic/SDW$_2$ phases, triatic/SDW$_3$ phases, and quartic phase.

At low magnetic field, we have found the vector chiral phase, marked by long-range vector chiral order and algebraically decaying incommensurate transverse-spin correlations. The vector chiral state is the quantum counterpart of the classical helical state. In the classical J_1-J_2 model the helical state appears as the ground state in the whole magnetization region, whereas in the spin-1/2 model the vector chiral phase appears only in the low-magnetization regime (but not at $M=0$). For larger magnetization, the chiral state is destroyed by the formation of quantum magnon bound states and turns into the spin-density-wave states.

At higher magnetic field, magnons form stable bound states caused by ferromagnetic attractive interactions. The stabilization of magnon bound states is a general feature of frustrated ferromagnets. Spin multipolar orders induced by the bound-state formation were discovered recently in spin-1/2 models on the square lattice,[54] the triangular lattice,[41] and the two-leg ladder lattice.[55] In all of these models, magnon bound states become stable when the ferromagnetic state is destroyed by competing antiferromagnetic and/or ring-exchange interactions. The unique feature of the present zigzag chain model is that the number of magnons forming a bound state increases consecutively with approaching the ferromagnetic phase boundary $J_1/J_2=-4$. This unique feature might relate to the fact that the zigzag spin chain with $J_1/J_2=-4$ has highly degenerate ground states.[37,38]

We have found various phases that can be well described by the effective theory for hard-core Bose gas of bound multimagnons. Near the saturation field, there appear various multipolar TL-liquid phases, such as the nematic (quadrupolar), triatic (octupolar), and quartic (hexadecapolar) phases, which are characterized by the condensation of bound multimagnons. With lowering the magnetic field from the saturation field, the increase in bound-magnon density enhances the effect of repulsion between bound magnons. This leads to a crossover from a high-field region of the multipolar TL liquids to a low-field region of spin-density-wave states, where density waves of bound multimagnons dominate.

Lastly we note that our phase diagram appears to be qualitatively consistent with the magnetic properties observed in the spin-1/2 chain cuprate $LiCuVO_4$, whose exchange couplings are estimated as $J_1/J_2\approx-0.4$ with ferromagnetic J_1.[11] Recent experiments revealed that, when a magnetic field is applied, the low-temperature phase undergoes two successive transitions with changing field.[12,13] Besides an usual spin-flop transition at $h_{c1}\approx 2.5$ T, which is presumably due to spin anisotropy effect, another magnetic phase transition occurs at $h_{c2}\approx 7.5$ T. Below h_{c2} (or more precisely in $h_{c1}<h<h_{c2}$), the low-temperature phase has spiral spin structure, having incommensurate spin order in the plane perpendicular to the applied field, as well as ferroelectricity.[14–16] In the field above h_{c2}, the system has a modulated magnetic order parallel to the field while the perpendicular spin components are disordered.[13] In comparison with the magnetic phase diagram of the J_1-J_2 model, it is natural to identify the magnetic transition at $h=h_{c2}$ with the transition between the vector chiral phase and the SDW_2 phase in our model (1). This means that the experimentally observed spin modulated state in high field can be characterized by a density-wave order of bound magnon pairs. Furthermore, in the light of our phase diagram, we predict that the nematic phase, which has not yet been observed experimentally, should appear in higher magnetic field. Further experimental studies on high magnetization phases would be interesting. On the theoretical side, it is important to include effects of interchain couplings, further interactions, and spin anisotropy to make more quantitative comparison between our theoretical results and experiments. In $LiCuVO_4$, the interchain coupling indeed induces three-dimensional order at very low temperature $T<T_N\approx 2.3$ K. We also note that the critical field h_{c2} is about 0.2 of the saturation field $h_s\approx 41$ T and considerably larger than the value estimated from the one-dimensional J_1-J_2 model.

Note added. Since the submission of this paper, a preprint by Sudan *et al.*[56] has appeared, in which a phase diagram very similar to ours is obtained independently. They have found a direct metamagnetic transition from the vector chiral phase to the ferromagnetic phase for large $|J_1|/J_2$ where bound states of $p\geq 5$ magnons are formed. In Sec. IV we discussed magnetization curves for $J_1/J_2\geq -3.6$ where only bound magnons of $p\leq 4$ participate in the magnetization process.

ACKNOWLEDGMENTS

It is our pleasure to acknowledge stimulating discussions with Shunsuke Furukawa, Shigeki Onoda, Masahiro Sato, and Oleg Starykh. This work was supported by Grants-in-Aid for Scientific Research from the Ministry of Education, Culture, Sports, Science and Technology (MEXT) of Japan (Grants No. 16GS0219, No. 17071011, No. 18043003, and No. 20046016), by the Next Generation Super Computing Project, Nanoscience Program, MEXT, Japan, and by Japan Society for Promotion of Science (Grant No. P06902). The numerical calculations were performed in part by using RIKEN Super Combined Cluster (RSCC).

APPENDIX: BLOCH THEOREM FOR SPIN CURRENT

In this appendix we prove that there is no net spin current flow in the ground state (even in the vector chiral phase). This is a variant of Bloch's theorem that there is no net current flow in the ground state without external field.[57–59]

We begin with defining the spin current. Since Hamiltonian (1) conserves the z component of the total spin $\Sigma_l \boldsymbol{s}_l$, the s^z current is a well-defined quantity. The equation of motion for s_l^z reads

$$\frac{\partial}{\partial t}s_l^z = -i[s_l^z,\mathcal{H}] = -J_1(\kappa_l^{(1)}-\kappa_{l-1}^{(1)}) - J_2(\kappa_l^{(2)}-\kappa_{l-2}^{(2)}), \tag{A1}$$

from which we deduce the s^z current flowing from the site l to the site $l+n$, which is given by $J_l^{(n)}=J_n\kappa_l^{(n)}$ $(n=1,2)$. It also follows from Eq. (A1) that

$$\frac{\partial}{\partial t}\sum_{m\leq l} s_m^z = -J_1\kappa_l^{(1)} - J_2(\kappa_l^{(2)}+\kappa_{l-1}^{(2)}), \tag{A2}$$

implying that the total s^z current flowing through the system is $J_{\mathrm{tot}}=J_1\kappa^{(1)}+2J_2\kappa^{(2)}$, where we have suppressed the site index l.

To prove our statement that the net current J_{tot} always vanishes in the ground state, we consider the J_1-J_2 spin chain of finite length L with the periodic boundary condition and add to its Hamiltonian $\mathcal{H}$ a weak symmetry-breaking term,

$$\mathcal{H}_y = -y\sum_l J_1\kappa_l^{(1)} \tag{A3}$$

with the coupling $y>0$. This term allows us to select a unique ground state with a broken Z_2 symmetry. Let us as-

sume that the unique ground state $|g\rangle_{L,y}$ has a nonvanishing expectation value of a linear combination of the vector chiralities,

$$\langle J_1\kappa_l^{(1)} + 2J_2\kappa_l^{(2)}\rangle_{L,y} > \frac{3y|J_1|}{4}, \tag{A4}$$

where $\langle\cdots\rangle_{L,y}$ is the average in the ground state $|g\rangle_{L,y}$.

We now introduce the twist operator

$$U_\theta = \exp\left(-i\sum_{l=1}^{L} l\theta s_l^z\right) \tag{A5}$$

with the twist angle $\theta=2\pi/L$. We then take $U_\theta|g\rangle_{L,y}$ as a trial state, which has a smaller net spin current than $|g\rangle_{L,y}$, and compare its energy with the energy of the assumed ground state $|g\rangle_{L,y}$. We find the energy difference

$$\begin{aligned}\Delta E &= \langle U_\theta^\dagger(\mathcal{H}+\mathcal{H}_y)U_\theta\rangle_{L,y} - \langle\mathcal{H}+\mathcal{H}_y\rangle_{L,y}\\ &= J_1(\cos\theta - 1)\sum_l \langle s_l^x s_{l+1}^x + s_l^y s_{l+1}^y - y\kappa_l^{(1)}\rangle_{L,y}\\ &\quad + J_2(\cos 2\theta - 1)\sum_l \langle s_l^x s_{l+2}^x + s_l^y s_{l+2}^y\rangle_{L,y}\\ &\quad - J_1\sin\theta\sum_l \langle \kappa_l^{(1)} + y(s_l^x s_{l+1}^x + s_l^y s_{l+1}^y)\rangle_{L,y}\\ &\quad - J_2\sin 2\theta\sum_l \langle\kappa_l^{(2)}\rangle_{L,y}.\end{aligned} \tag{A6}$$

Assuming the translation invariance of the ground state, we reduce Eq. (A6) to

$$\begin{aligned}\Delta E = &-2\pi\langle J_1\kappa_l^{(1)} + 2J_2\kappa_l^{(2)}\rangle_{L,y} - 2\pi y J_1\langle s_l^x s_{l+1}^x + s_l^y s_{l+1}^y\rangle_{L,y}\\ &+ \mathcal{O}(L^{-1})\end{aligned} \tag{A7}$$

for $L\gg 1$. Using the inequality $-J_1\langle s_l^x s_{l+1}^x + s_l^y s_{l+1}^y\rangle_{L,y} < \frac{3}{4}|J_1|$, we conclude from Eqs. (A4) and (A7) that $\Delta E<0$. This is in contradiction with the assumption of $|g\rangle_{L,y}$ being the ground state. This means that our assumption (A4) is not valid and instead we have

$$\langle J_1\kappa_l^{(1)} + 2J_2\kappa_l^{(2)}\rangle_{L,y} \le \alpha y, \tag{A8}$$

where α is a positive constant ($\alpha=3|J_1|/4$).

In the same way, starting from the assumption that the ground state $|g\rangle_{L,y}$ has a negative net current, $\langle J_1\kappa_l^{(1)} + 2J_2\kappa_l^{(2)}\rangle_{L,y} < -\frac{3}{4}y|J_1|$, and using the twisted trial state $U_\theta|g\rangle_{L,y}$ with the angle $\theta=-2\pi/L$, we can again show that the trial state has a lower energy than the assumed ground state, and thereby we have $\langle J_1\kappa_l^{(1)} + 2J_2\kappa_l^{(2)}\rangle_{L,y} \ge -\alpha y$. We thus obtain

$$|\langle J_1\kappa_l^{(1)} + 2J_2\kappa_l^{(2)}\rangle_{L,y}| \le \alpha y. \tag{A9}$$

We now take the limit $L\to\infty$ and then $y\to 0$, yielding

$$J_1\langle\kappa_l^{(1)}\rangle + 2J_2\langle\kappa_l^{(2)}\rangle = 0. \tag{A10}$$

It is straightforward to generalize this identity to the case when the ground state breaks translation symmetry as well as to other spin Hamiltonians.

[1] A. V. Chubukov, Phys. Rev. B **44**, 4693 (1991).
[2] D. C. Cabra, A. Honecker, and P. Pujol, Eur. Phys. J. B **13**, 55 (2000).
[3] F. Heidrich-Meisner, A. Honecker, and T. Vekua, Phys. Rev. B **74**, 020403(R) (2006).
[4] D. V. Dmitriev and V. Ya. Krivnov, Phys. Rev. B **73**, 024402 (2006).
[5] R. O. Kuzian and S.-L. Drechsler, Phys. Rev. B **75**, 024401 (2007).
[6] L. Kecke, T. Momoi, and A. Furusaki, Phys. Rev. B **76**, 060407(R) (2007).
[7] T. Vekua, A. Honecker, H.-J. Mikeska, and F. Heidrich-Meisner, Phys. Rev. B **76**, 174420 (2007).
[8] S. Furukawa, M. Sato, Y. Saiga, and S. Onoda, arXiv:0802.3256 (unpublished).
[9] H. Katsura, S. Onoda, J. H. Han, and N. Nagaosa, arXiv:0804.0669 (unpublished).
[10] M. Hase, H. Kuroe, K. Ozawa, O. Suzuki, H. Kitazawa, G. Kido, and T. Sekine, Phys. Rev. B **70**, 104426 (2004).
[11] M. Enderle, C. Mukherjee, B. Fåk, R. K. Kremer, J.-M. Broto, H. Rosner, S.-L. Drechsler, J. Richter, J. Malek, A. Prokofiev, W. Assmus, S. Pujol, J.-L. Raggazzoni, H. Rakoto, M. Rheinstädter, and H. M. Rønnow, Europhys. Lett. **70**, 237 (2005).
[12] M. G. Banks, F. Heidrich-Meisner, A. Honecker, H. Rakoto, J.-M. Broto, and R. K. Kremer, J. Phys.: Condens. Matter **19**, 145227 (2007).
[13] N. Büttgen, H. A. Krug von Nidda, L. E. Svistov, L. A. Prozorova, A. Prokofiev, and W. Aßmus, Phys. Rev. B **76**, 014440 (2007).
[14] Y. Naito, K. Sato, Y. Yasui, Y. Kobayashi, Y. Kobayashi, and M. Sato, J. Phys. Soc. Jpn. **76**, 023708 (2007).
[15] Y. Yasui, Y. Naito, K. Sato, T. Moyoshi, M. Sato, and K. Kakurai, J. Phys. Soc. Jpn. **77**, 023712 (2008).
[16] F. Schrettle, S. Krohns, P. Lunkenheimer, J. Hemberger, N. Büttgen, H.-A. Krug von Nidda, A. V. Prokofiev, and A. Loidl, Phys. Rev. B **77**, 144101 (2008).
[17] C. K. Majumdar and D. K. Ghosh, J. Math. Phys. **10**, 1388 (1969).
[18] C. K. Majumdar and D. K. Ghosh, J. Math. Phys. **10**, 1399 (1969).
[19] F. D. M. Haldane, Phys. Rev. B **25**, 4925 (1982).
[20] R. Jullien and F. D. M. Haldane, Bull. Am. Phys. Soc. **28**, 344 (1983).
[21] K. Okamoto and K. Nomura, Phys. Lett. A **169**, 433 (1992).
[22] S. Eggert, Phys. Rev. B **54**, R9612 (1996).
[23] S. R. White and I. Affleck, Phys. Rev. B **54**, 9862 (1996).
[24] K. Okunishi, Y. Hieida, and Y. Akutsu, Phys. Rev. B **60**, R6953 (1999).
[25] K. Okunishi and T. Tonegawa, J. Phys. Soc. Jpn. **72**, 479 (2003).
[26] A. A. Nersesyan, A. O. Gogolin, and F. H. L. Eßler, Phys. Rev.

Lett. **81**, 910 (1998).
[27] M. Kaburagi, H. Kawamura, and T. Hikihara, J. Phys. Soc. Jpn. **68**, 3185 (1999).
[28] T. Hikihara, M. Kaburagi, and H. Kawamura, Phys. Rev. B **63**, 174430 (2001).
[29] A. Kolezhuk and T. Vekua, Phys. Rev. B **72**, 094424 (2005).
[30] I. P. McCulloch, R. Kube, M. Kurz, A. Kleine, U. Schollwöck, and A. K. Kolezhuk, Phys. Rev. B **77**, 094404 (2008).
[31] K. Okunishi, arXiv:0805.3872 (unpublished).
[32] T. Hikihara, T. Momoi, A. Furusaki, and H. Kawamura (unpublished).
[33] S. R. White, Phys. Rev. Lett. **69**, 2863 (1992).
[34] S. R. White, Phys. Rev. B **48**, 10345 (1993).
[35] U. Schollwöck, Rev. Mod. Phys. **77**, 259 (2005).
[36] K. A. Hallberg, Adv. Phys. **55**, 477 (2006).
[37] T. Hamada, J. Kane, S. Nakagawa, and Y. Natsume, J. Phys. Soc. Jpn. **57**, 1891 (1988).
[38] T. Tonegawa and I. Harada, J. Phys. Soc. Jpn. **58**, 2902 (1989).
[39] The existence of a vector chiral phase was also established by recent numerical studies for the antiferromagnetic J_1-J_2 spin chain (Refs. 30–32).
[40] A. F. Andreev and I. A. Grishchuk, Sov. Phys. JETP **60**, 267 (1984).
[41] T. Momoi, P. Sindzingre, and N. Shannon, Phys. Rev. Lett. **97**, 257204 (2006).
[42] Á. Rapp, G. Zaránd, C. Honerkamp, and W. Hofstetter, Phys. Rev. Lett. **98**, 160405 (2007).
[43] S. Capponi, G. Roux, P. Lecheminant, P. Azaria, E. Boulat, and S. R. White, Phys. Rev. A **77**, 013624 (2008).
[44] G. Roux, S. Capponi, P. Lecheminant, and P. Azaria, arXiv:0807.0412 (unpublished).
[45] T. Hikihara and A. Furusaki, Phys. Rev. B **63**, 134438 (2001).
[46] T. Hikihara and A. Furusaki, Phys. Rev. B **69**, 064427 (2004).
[47] F. D. M. Haldane, Phys. Rev. Lett. **45**, 1358 (1980).
[48] N. M. Bogoliubov, A. G. Izergin, and V. E. Korepin, Nucl. Phys. B **275**, 687 (1986).
[49] D. C. Cabra, A. Honecker, and P. Pujol, Phys. Rev. B **58**, 6241 (1998).
[50] The rapid decrease in the vector chiral correlation functions at $r \gtrsim 80$ is an open boundary effect. The bosonic field $\phi_i(x)$ obeys the Dirichlet boundary condition (ϕ=const) at the boundaries. This is not compatible with the vector chiral order which requires the dual bosonic field $\theta_-(x)$ to be fixed.
[51] In the Ising limit a similar hard-core boson theory was used to describe the intermediate phase between the fully polarized state and (2,2) antiphase state by J. Igarashi, J. Phys. Soc. Jpn. **58**, 4600 (1989); T. Tonegawa, I. Harada, and J. Igarashi, Prog. Theor. Phys. Suppl. **101**, 513 (1990).
[52] T. Giamarchi, *Quantum Physics in One Dimension* (Clarendon, Oxford, 2004).
[53] The slow convergence of the DMRG calculation should be ascribed to the presence of many low-lying states in small energy scale due to the strong frustration at $J_1/J_2 \to -4$.
[54] N. Shannon, T. Momoi, and P. Sindzingre, Phys. Rev. Lett. **96**, 027213 (2006).
[55] T. Hikihara and S. Yamamoto, J. Phys. Soc. Jpn. **77**, 014709 (2008).
[56] J. Sudan, A. Lüscher, and A. M. Läuchli, arXiv:0807.1923 (unpublished).
[57] D. Bohm, Phys. Rev. **75**, 502 (1949).
[58] Y. Ohashi and T. Momoi, J. Phys. Soc. Jpn. **65**, 3254 (1996).
[59] N. Bray-Ali and Z. Nussinov, arXiv:0803.0984 (unpublished).